BSC

Design Calculation or Analysis Cover Sheet

Complete only applicable items.

1. QA: QA
2. Page 1 of 63

3. System	4. Document Identifier
Monitored Geologic Repository	000-00C-MGR0-01400-000-00B

5. Title

Nonlithophysal Rock Fall on Waste Packages

6. Group

Thermal Structural Analysis

7. Document Status Designation

☐ Preliminary ☒ Committed ☐ Confirmed ☐ Cancelled/Superseded

8. Notes/Comments

This calculation is a revision of "Rock Fall on Waste Packages", 000-00C-MGR0-01400-000-00A, a committed calculation.

Attachments	Total Number of Pages
Attachment I. Directory Listing (data DVD) of Electronic Files	2
Attachment II. Figures obtained from LS-DYNA	3
Attachment III. Data DVD Attachment, Electronic Files	N/A

RECORD OF REVISIONS

9. No.	10. Reason For Revision	11. Total # of Pgs.	12. Last Pg. #	13. Originator (Print/Sign/Date)	14. Checker (Print/Sign/Date)	15. EGS (Print/Sign/Date)	16. Approved/Accepted (Print/Sign/Date)
00A	Initial Issue	75	II-7	Zekai Ceylan	Kenneth Jaquay	Michael J. Anderson	Michael J. Anderson 2/17/2004
ECN1	Change status to committed	1	1	Tim Schmitt	Michael Mullin	Michael J. Anderson	Michael J. Anderson 3/12/2005
00B	Extensive revisions to entire text, all pages are affected. Update calculation to match Basis of Design and new credible bounding rock.	63	63	Bryan Dunlap 7/24/07	Kenneth Jaquay 7/24/07	Jason Viggato 7/24/07	Michael J. Anderson 7/24/07

DISCLAIMER

The calculations contained in this document were developed by Bechtel SAIC Company, LLC (BSC) and are intended solely for the use of BSC in its work for the Yucca Mountain Project.

CONTENTS

Page

FIGURE

Page

TABLES

Page

ACRONYMS

BWR	Boiling Water Reactor
CSNF	Commercial Spent Nuclear Fuel
DHLW	Defense High Level Waste
DOE	U.S. Department of Energy
EP	Emplacement Pallet
EWA	Element Wall-Averaged
FE	Finite Element
FER	Finite Element Representation
J	Joules (Energy, Newton·meter)
MT	Metric Ton (1,000 kilograms)
MPa	Mega Pascal (force per unit area)
OCB	Outer Corrosion Barrier
PWR	Pressurized Water Reactor
RT	Room Temperature
SI	Stress Intensity
SNF	Spent Nuclear Fuel
SS	Stainless Steel
TAD	Transportation, Aging, and Disposal
WP	Waste Package

1. PURPOSE

The purpose of this calculation is to determine the following:

- The pre-closure structural response of emplaced waste packages (WPs) to Nonlithophysal (large intact rock) rock falls during design basis event dynamic loads. Considering:
  - Transportation, Aging and Disposal (TAD) canister bearing WP (TAD bearing WP will have the same response to rock fall as Naval Canister bearing WPs).
  - 5DHLW/DOE Co-disposal short WP (Co-disposal WP).
  - All WPs analyzed wh`ile resting on an emplacement pallet (EP).
  - All WPs analyzed with a reduction of thickness of the Outer Corrosion Barrier (OCB) components, assuming a conservative level of corrosion during the preclosure period.
- The bounding credible rock fall scenario will be analyzed at several different locations on the WP to determine the maximum OCB stresses.
  - Considerations for multiple rocks striking the same location.
  - Considerations for ground support:
    - Rockbolt in bounding credible rock at point of impact
    - Multiple rock impact due to rockbolt holding expected size rocks together.
- The scope of the calculation is limited to reporting the structural response of the WPs OCB in the form of stress intensities. If failure criterion screening using the calculated stress intensities in the OCB are not met then the OCB is considered breached and the WP is considered failed.
- This calculation is intended for use in support of the committed design activities for the license application designs of the WPs.

2. REFERENCES

2.1 PROCEDURES/DIRECTIVES

2.1.1 EG-PRO-3DP-G04B-00037, Rev. 8. *Calculations and Analyses*. Las Vegas, Nevada: Bechtel SAIC Company. ACC: ENG.20070420.0002

2.1.2 IT-PRO-0011, Rev. 5, ICN 0. *Software Management.* Las Vegas, NV: Bechtel SAIC Company. ACC: DOC.20070521.0001.

2.1.3 ORD (Office of Repository Development) 2007. *Repository Project Management Automation Plan*. 000-PLN-MGR0-00200-000, Rev. 00E. Las Vegas, Nevada: U.S. Department of Energy, Office of Repository Development. ACC: ENG.20070326.0019.

2.1.4. CC-PRO-2001, Rev 3. *Technical Interface Control*. Las Vegas, Nevada: Bechtel SAIC Company. ACC: DOC.20070423.0002.

2.2 DESIGN INPUTS

2.2.1. Dieter, G.E. 1976. *Mechanical Metallurgy*. 2nd Edition. Materials Science and Engineering Series. New York, New York: McGraw-Hill Book Company. TIC: 247879. ISBN: 0-07-016891-1.

2.2.2. ASM (American Society for Metals) 1980. *Properties and Selection: Stainless Steels, Tool Materials and Special-Purpose Metals*. Volume 3 of *Metals Handbook*. 9th Edition. Benjamin, D., ed. Metals Park, Ohio: American Society for Metals. TIC: 209801. ISBN: 0-87170-009-3.

2.2.3. ASME (American Society of Mechanical Engineers) 2001. *2001 ASME Boiler and Pressure Vessel Code (includes 2002 addenda)*. New York, New York: American Society of Mechanical Engineers. TIC: 251425.

2.2.4. ASTM G 1-90 (Reapproved 1999). 1999. *Standard Practice for Preparing, Cleaning, and Evaluating Corrosion Test Specimens*. West Conshohocken, Pennsylvania: American Society for Testing and Materials. TIC: 238771.

2.2.5. BSC (Bechtel SAIC Company) 2007. *Ground Control for Emplacement Drifts for LA*. 800-K0C-SSE0-00100-000-00B. Las Vegas, Nevada: Bechtel SAIC Company. ACC: ENG.20070425.0001.

2.2.6. Boyer, H.E., ed. 2000. *Atlas of Stress-Strain Curves*. Metals Park, Ohio: ASM International. TIC: 248901. ISBN: 0-87170-240-1.

2.2.7. LL020603612251.015. Slow Strain Rate Test Generated Stress Corrosion Cracking Data. Submittal date: 08/27/2002.

2.2.8. Haynes International. 1997. Hastelloy C-22 Alloy. Kokomo, Indiana: Haynes International. TIC: 238121.

2.2.9. Avallone, E.A. and Baumeister, T., III, eds. 1987. *Marks' Standard Handbook for Mechanical Engineers*. 9th Edition. New York, New York: McGraw-Hill. TIC: 206891. ISBN: 0-07-004127.

2.2.10. Meriam, J.L. and Kraige, L.G. 1987. *Statics*. Volume 1 of *Engineering Mechanics*. 2nd Edition. Pages 441, 443. New York, New York: John Wiley & Sons. TIC: 241293.

2.2.11. Beer, F.P. and Johnston, E.R., Jr. 1977. *Vector Mechanics for Engineers, Statics*. 3rd Edition. New York, New York: McGraw-Hill Book Company. TIC: 247391. ISBN: 0-07-004278-0.

2.2.12. BSC (Bechtel SAIC Company) 2004. *Drip Shield Structural Response to Rock Fall*.

000-00C-SSE0-00300-000-00A. Las Vegas, Nevada: Bechtel SAIC Company. ACC: ENG.20040405.0019; ENG.20050817.0026.

2.2.13. Not used

2.2.14. Not used.

2.2.15. Stout, R.B. and Leider, H.R., eds. 1997. *Waste Form Characteristics Report Revision 1.* UCRL-ID-108314. Version 1.2. Livermore, California: Lawrence Livermore National Laboratory. ACC: MOL.19980512.0133.

2.2.16. BSC (Bechtel SAIC Company) 2006. *Basis of Design for the TAD Canister-Based Repository Design Concept.* 000-3DR-MGR0-00300-000-000. Las Vegas, Nevada: Bechtel SAIC Company. ACC: ENG.20061023.0002.

2.2.17. BSC (Bechtel SAIC Company) 2007. *IED GEOTECHNICAL AND THERMAL PARAMETERS IV*. 800-IED-MGR0-00404-000-00A. Las Vegas, Nevada: BSC. ACC: ENG.20070125.0018.

2.2.18. BSC (Bechtel SAIC Company) 2004. *Commercial SNF Waste Package Design Report.* 000-00C-DSU0-02800-000-00B. Las Vegas, Nevada: Bechtel SAIC Company. ACC: ENG.20040709.0001; ENG.20050817.0021.

2.2.19. ASM International 1990. *Properties and Selection: Irons, Steels, and High-Performance Alloys*. Volume 1 of *Metals Handbook.* 10th Edition. Materials Park, Ohio: ASM International. TIC: 245666. ISBN: 0-87170-377-7.

2.2.20. Jaeger, J.C. and Cook, N.G.W. 1979. *Fundamentals of Rock Mechanics*. 3rd Edition. New York, New York: Chapman and Hall. TIC: 218325. ISBN: 0-41222010-5.

2.2.21. Chen, W.F. 1982. *Plasticity in Reinforced Concrete.* New York, New York: McGraw-Hill. TIC: 240453. ISBN: 0-07-010687-8.

2.2.22. BSC (Bechtel SAIC Company) 2005. *Q-List.* 000-30R-MGR0-00500-000-003. Las Vegas, Nevada: Bechtel SAIC Company. ACC: ENG.20050929.0008.

2.2.23. LS-DYNA V. 970.3858 D MPP. 2003. HP-UX 11.22. STN: 10300-970.3858 D MPP-00.

2.2.24. Mecham, D.C., ed. 2004. *Waste Package Component Design Methodology Report.* 000-30R-WIS0-00100-000-002. Las Vegas, Nevada: Bechtel SAIC Company. ACC: ENG.20040713.0003.

2.2.25. BSC (Bechtel SAIC Company) 2007. *IED Emplacement Pallet.* 800-IED-SSE0-00201-000-00B. Las Vegas, Nevada: Bechtel SAIC Company. ACC: ENG.20070608.0007.

2.2.26. DOE (U.S. Department of Energy) 2007. *"High-Level Radioactive Waste and U.S. Department of Energy and Naval Spent Nuclear Fuel to the Civilian Radioactive Waste*

Management System." Volume 1 of *Integrated Interface Control Document.* DOE/RW-0511, Rev. 3. Washington, D.C.: U.S. Department of Energy, Office of Civilian Radioactive Waste Management. ACC: DOC.20070125.0002.

2.2.27. DOE (U.S. Department of Energy) 2003. *Validation Test Report for LS-DYNA Version 970.3858 D MPP.* 10300-VTR-970.3858 D MPP-00. Las Vegas, Nevada: U.S. Department of Energy, Office of Repository Development. ACC: MOL.20031218.0337.

2.2.28. BSC (Bechtel SAIC Company) 2007. *Probabilistic Characterization of Preclosure Rockfalls in Emplacement Drifts.* 800-00C-MGR0-00300-000-00A. Las Vegas, Nevada: Bechtel SAIC Company. ACC: ENG.20070329.0009.

2.2.29. Stillborg, B. 1994. *Professional Users Handbook for Rock Bolting.* Series on Rock and Soil Mechanics Volume 18. 2nd Edition. Clausthal-Zellerfield, Germany: Trans Tech Publications. TIC: 253370.

2.2.30. BSC (Bechtel SAIC Company) 2007. *TAD Waste Package Configuration.* 000-MW0-DSC0-00101-000 REV 00B. Las Vegas, Nevada: Bechtel SAIC Company. ACC: ENG.20070301.0010.

2.2.31. BSC (Bechtel SAIC Company) 2007. *TAD Waste Package Configuration.* 000-MW0-DSC0-00102-000 REV 00B. Las Vegas, Nevada: Bechtel SAIC Company. ACC: ENG.20070301.0011.

2.2.32. BSC (Bechtel SAIC Company) 2007. *TAD Waste Package Configuration.* 000-MW0-DSC0-00103-000 REV 00B. Las Vegas, Nevada: Bechtel SAIC Company. ACC: ENG.20070301.0012.

2.2.33. BSC (Bechtel SAIC Company) 2004. *Design and Engineering, Emplacement Pallet Assembly Exploded [Sheet 2 of 15].* 000-M00-SSE0-00302-000-00A. Las Vegas, Nevada: Bechtel SAIC Company. ACC: ENG.20040224.0006.

2.2.34. BSC (Bechtel SAIC Company) 2004. *Design and Engineering, Emplacement Pallet Waste Package Support Assembly Exploded [Sheet 3 of 15].* 000-M00-SSE0-00303-000-00A. Las Vegas, Nevada: Bechtel SAIC Company. ACC: ENG.20040224.0007.

2.2.35. BSC (Bechtel SAIC Company) 2004. *Design and Engineering, Emplacement Pallet Assembly Plate 1 [Sheet 4 of 15].* 000-M00-SSE0-00304-000-00A. Las Vegas, Nevada: Bechtel SAIC Company. ACC: ENG.20040224.0008.

2.2.36. BSC (Bechtel SAIC Company) 2004. *Design and Engineering, Emplacement Pallet Assembly Plate 2 [Sheet 5 of 15].* 000-M00-SSE0-00305-000-00A. Las Vegas, Nevada: Bechtel SAIC Company. ACC: ENG.20040224.0009.

2.2.37. BSC (Bechtel SAIC Company) 2004. *Design and Engineering Emplacement Pallet Assembly Plate 3 [Sheet 6 of 15].* 000-M00-SSE0-00306-000-00A. Las Vegas, Nevada: Bechtel SAIC Company. ACC: ENG.20040224.0010.

2.2.38. BSC (Bechtel SAIC Company) 2004. *Design and Engineering, Emplacement Pallet Assembly Plate 4 [Sheet 7 of 15]*. 000-M00-SSE0-00307-000-00A. Las Vegas, Nevada: Bechtel SAIC Company. ACC: ENG.20040224.0011.

2.2.39. BSC (Bechtel SAIC Company) 2004. *Design and Engineering, Emplacement Pallet Assembly Plate 5 [Sheet 8 of 15]*. 000-M00-SSE0-00308-000-00A. Las Vegas, Nevada: Bechtel SAIC Company. ACC: ENG.20040224.0012.

2.2.40. BSC (Bechtel SAIC Company) 2004. *Design and Engineering, Emplacement Pallet Assembly Plate 6 [Sheet 9 of 15]*. 000-M00-SSE0-00309-000-00A. Las Vegas, Nevada: Bechtel SAIC Company. ACC: ENG.20040224.0013.

2.2.41. BSC (Bechtel SAIC Company) 2004. *Design and Engineering, Emplacement Pallet Assembly Plate 7 [Sheet 10 of 15]*. 000-M00-SSE0-00310-000-00A. Las Vegas, Nevada: Bechtel SAIC Company. ACC: ENG.20040224.0014.

2.2.42. BSC (Bechtel SAIC Company) 2004. *Design and Engineering, Emplacement Pallet Assembly Plate 8 [Sheet 11 of 15]*. 000-M00-SSE0-00311-000-00A. Las Vegas, Nevada: Bechtel SAIC Company. ACC: ENG.20040224.0015.

2.2.43. BSC (Bechtel SAIC Company) 2004. *Design and Engineering, Emplacement Pallet Assembly Plate 9 [Sheet 12 of 15]*. 000-M00-SSE0-00312-000-00A. Las Vegas, Nevada: Bechtel SAIC Company. ACC: ENG.20040224.0016.

2.2.44. BSC (Bechtel SAIC Company) 2004. *Design and Engineering, Emplacement Pallet Assembly Tube 1 [Sheet 13 of 15]*. 000-M00-SSE0-00313-000-00A. Las Vegas, Nevada: Bechtel SAIC Company. ACC: ENG.20040224.0017.

2.2.45. BSC (Bechtel SAIC Company) 2004. *Design and Engineering, Emplacement Pallet Assembly Tube 2 [Sheet 14 of 15]*. 000-M00-SSE0-00314-000-00A. Las Vegas, Nevada: Bechtel SAIC Company. ACC: ENG.20040224.0018.

2.2.46. BSC (Bechtel SAIC Company) 2004. *Design and Engineering, Emplacement Pallet Assembly Tube 3 [Sheet 15 of 15]*. 000-M00-SSE0-00315-000-00A. Las Vegas, Nevada: Bechtel SAIC Company. ACC: ENG.20040224.0019.

2.2.47. BSC (Bechtel SAIC Company) 2007. *5-DHLW/DOE SNF - Short Co-Disposal Waste Package Configuration.* 000-MW0-DS00-00101-000 REV 00C. Las Vegas, Nevada: Bechtel SAIC Company. ACC: ENG.20070306.0003.

2.2.48. BSC (Bechtel SAIC Company) 2007. *5-DHLW/DOE SNF - Short Co-Disposal Waste Package Configuration.* 000-MW0-DS00-00102-000 REV 00B. Las Vegas, Nevada: Bechtel SAIC Company. ACC: ENG.20070205.0006.

2.2.49. BSC (Bechtel SAIC Company) 2007. *5-DHLW/DOE SNF - Short Co-Disposal Waste Package Configuration.* 000-MW0-DS00-00103-000 REV 00B. Las Vegas, Nevada: Bechtel SAIC Company. ACC: ENG.20070205.0007.

2.2.50. BSC (Bechtel SAIC Company) 2005. *21-PWR Site-Specific Canister / Basket Guide Location and Orientation.* 000-M00-HA00-00104-000-00B. Las Vegas, Nevada: Bechtel SAIC Company. ACC: ENG.20050613.0021.

2.2.51. BSC (Bechtel SAIC Company) 2005. *21-PWR Site-Specific Canister / Basket Fuel Basket Assembly Detail Drawing.* 000-M00-HA00-00106-000-00B. Las Vegas, Nevada: Bechtel SAIC Company. ACC: ENG.20050613.0023.

2.2.52. BSC (Bechtel SAIC Company) 2005. *21-PWR Site-Specific Canister / Basket Fuel Tube Assembly Detail Drawing.* 000-M00-HA00-00107-000-00B. Las Vegas, Nevada: Bechtel SAIC Company. ACC: ENG.20050613.0024.

2.2.53. Nicholas, T. 1980. *Dynamic Tensile Testing of Structural Materials Using A Split Hopkinson Bar Apparatus.* AFWAL-TR-80-4053. Wright-Patterson Air Force Base, Ohio: Air Force Wright Aeronautical Laboratories. TIC: 249469.

2.2.54. Roark, R.J. and Young, W.C. 1975. *Formulas for Stress and Strain.* 5th Edition. New York, New York: McGraw-Hill. TIC: 240746. ISBN: 0-07-053031-9.

2.2.55. BSC (Bechtel SAIC Company) 2007. *Quality Management Directive.* QA-DIR-10 Rev.001. Las Vegas, Nevada: Bechtel SAIC Company, ACC: ENG.20070330.0001.

2.2.56. BSC (Bechtel SAIC Company) 2005. *IED WASTE PACKAGE PROCESSES, GROUND MOTION TIME HISTORIES, AND TESTING AND MATERIALS [Sheet 1 of 1].* 800-IED-WIS0-00501-000-00A. Las Vegas, Nevada: Bechtel SAIC Company, ACC: ENG.20050406.0004.

2.2.57. BSC (Bechtel SAIC Company) 2007. *8th Meeting of the Waste Package Design Change Control Board.* 000-G17-GETS-00008. Las Vegas, Nevada: Bechtel SAIC Company. ACC: ENG.20070104.0011.

2.2.58. BSC (Bechtel SAIC Company) 2004. *21-PWR Waste Package Configuration.* 000-MW0-DSU0-00401-000-00D. Las Vegas, Nevada: Bechtel SAIC Company. ACC: ENG.20040708.0004.

2.2.59. BSC (Bechtel SAIC Company) 2004. *21-PWR Waste Package Configuration.* 000-MW0-DSU0-00402-000-00B. Las Vegas, Nevada: Bechtel SAIC Company. ACC: ENG.20040119.0004.

2.2.60. BSC (Bechtel SAIC Company) 2004. *21-PWR Waste Package Configuration.* 000-MW0-DSU0-00403-000-00D. Las Vegas, Nevada: Bechtel SAIC Company. ACC: ENG.20040708.0005.

2.2.61. DOE (U.S. Department of Energy) 2007. *Transportation, Aging and Disposal Canister System Performance Specification.* WMO-TADCS-000001, Rev. 0. DOE/RW-0585. Washington D.C.: U.S. Department of Energy, Office of Civilian Radioactive Waste Management. ACC: DOC.20070614.0007.

2.2.62. BSC (Bechtel SAIC Company) 2004. *Horizontal Drop of Naval SNF Long Waste Package.* 000-00C-DNF0-01000-000-00A. Las Vegas, Nevada: Bechtel SAIC Company. ACC: ENG.20040301.0012.

2.2.63. BSC (Bechtel SAIC Company) 2005. *5-DHLW/DOE SNF - Long Waste Package Tip-over from Elevated Surface.* 000-00C-DS00-00400-000-00A. Las Vegas, Nevada: Bechtel SAIC Company. ACC: ENG.20050214.0006.

2.3 DESIGN CONSTRAINTS

None

2.4 DESIGN OUTPUTS

Results from this calculation will be used by Subsurface Engineering Organization calculations and analyses.

Results from this calculation are expected to be used in a revision or superseding IED of *IED STRUCTURAL RESPONSE OF ENGINEERED BARRIER SYSTEM COMPONENTS TO NORMAL LOADS AND TO DISRUPTIVE EVENTS*, 800-IED-WIS0-02001-000-00A, ENG.20060925.0005.

3. ASSUMPTIONS

3.1 ASSUMPTIONS REQUIRING VERIFICATION

3.1.1 Waste Package and Emplacement Pallet Dimensions and Materials

The dimensions, masses, materials and load paths of the waste package (WP) and emplacement pallet (EP) used in the development of this calculation, corresponding to the drawings and sketches of Reference 2.2.30 to 2.2.52, are assumed to be reasonably the same in the region of high stress as the final definitive design.

Rationale–The rationale for this assumption is that the design of References 2.2.30 to 2.2.52 in the region of high stress is representative of the design created for the License Application (LA). The majority of the analyses use a WP sleeve design that includes machining for the attachment of a trunnion collar (References 2.2.58 to 2.2.60) which is conservative when compared to the WP sleeve design without the removal of material due to machining (References 2.2.30 to 2.2.32). Analyses that include the WP sleeve design without machining were included to confirm the conservativeness of this assumption. The WP sleeve design that includes machining material away for the attachment of a trunnion collar has been superseded, and the reference configuration drawings, References 2.2.58 thru 2.2.60, have been cancelled. The superseded WP sleeve design was used in these analyses in order to calculate conservative OCB stress intensities due to rock falls on the WP sleeves. This assumption is used in Sections 6.1 and 6.5 and will require verification at completion of the final definitive design. This assumption is being tracked in CalcTrac.

3.1.2 TAD Canister Dimensions and Materials

The geometry, dimensions and mass of the loaded TAD SNF canister are assumed to be the same as the loaded Naval SNF Long canister. The material used to model the TAD SNF canister is Type 316L Stainless Steel (SS), which is a 300 Series stainless steel as specified in Reference 2.2.61, Section 3.1.8. Additional analyses where other 300 Series stainless steels are modeled as the material of the TAD canister are not required to determine the peak structural response in the OCB.

Rationale- The rationale for this assumption is that the dimensions of the TAD SNF and Naval SNF Long canisters will be similar (Ref. 2.2.16, Section 11.2.2.3) and the mass of the loaded canisters will have negligible effect on the results of this calculation. Which 300 Series stainless steel the TAD canister will be constructed of has not been finalized, and it cannot be predetermined that 316L SS would be a conservative material selection or not. However, because the TAD canister is surrounded by the 2 inch thick inner vessel and the 1 inch thick OCB, the sensitivity of the OCB structural response to rock fall due to which 300 Series stainless steel the TAD canister is constructed of is expected to be small. This assumption is used in Sections 6.1 and 6.2 and will require verification at completion of the final definitive design. This assumption is being tracked in CalcTrac.

3.1.3 Rockbolt Type Selected for Emplacement Drift Ground Support

The current ground support design in the emplacement drifts calls for the use of Super Swellex rockbolts. It is assumed that the Super Swellex rockbolts will be used in the final emplacement drift ground support design for the LA submittal.

Rationale-The Super Swellex rockbolts are the preferred friction-type rockbolt system in the current design for the emplacement drift ground support (Reference 2.2.5, Sections 6.6.1, 6.7.2.2 and 7), there is no expectation that the preference for the Swellex rockbolt system will change before the LA submittal. This assumption is used in Section 6.5.1 and will require verification at completion of the final definitive design. This assumption is being tracked in CalcTrac.

3.2 ASSUMPTIONS NOT REQUIRING VERIFICATION

3.2.1 Material Properties and Temperature Dependency

Room temperature (RT) (20 °C (68 °F)) material property values are assumed for the Outer Corrosion Barrier (OCB), Inner Vessel, and EP for all analyses. The impact of using RT values for these material properties is anticipated to be small.

Rationale– All temperature dependent event sequence results to date show slightly higher damage (stress intensity ratio to allowable) in the OCB when using the RT property values compared to property values for temperatures up to 300 °C (572 °F), e.g. References 2.2.62 and 2.2.63 (included for historical purposes). Therefore this assumption does not require verification. This assumption is used in Section 6.1.

3.2.2 Material Properties for the Rock

The temperature-dependent material properties are not published in traditional sources (e.g., The ASTM, ASME and ASM standards, codes, and material property data) for TSw2 (Topopah Spring welded tuff, nonlithophysal) rock except at RT. The corresponding RT material properties are assumed for this material. The impact of using RT material properties is anticipated to be small.

Rationale– The material properties in question do not have dominant impact on the calculation results. The likely exception is the yield strength of the rock, which decreases with the increasing temperature. Thus, the representation of the rock as an elastic-ideally-plastic solid with room temperature yield strength is conservative. Therefore this assumption does not require verification. This assumption is used in Section 6.1 and corresponds to Section 5.2.16.1 in Reference 2.2.24.

3.2.3 Metallic Material Properties and Rate Dependency

Some of the rate-dependent material properties are not available for the metallic materials used at any strain rate. The material properties obtained under the static loading conditions are assumed for all materials. The impact of using material properties obtained under static loading conditions is anticipated to be small.

Rationale– The mechanical properties of subject materials do not significantly change at the maximum wall-averaged strain rates that occur during the worst case rock fall. Figure 1 is a time plot in seconds (s) of the wall-averaged effective plastic strain at the OCB location with the highest wall-averaged stress intensity during the worst case rock fall scenario without a rockbolt (see section 7.2). From Figure 1 the maximum wall-averaged effective plastic strain rate (maximum slope of the plastic strain curve) is seen to be = 0.0211/0.001 s = 21 s^{-1}. For this value of strain rate, Reference 2.2.53 Figures 27 and 30, pages 42 and 45, respectively, indicates only a minor strengthening of 300 Series stainless steel and high alloy steels. Therefore, the impact of using material properties obtained under static loading conditions will be small and this assumption will not require verification. This assumption is used in Section 6.1 and corresponds to Section 5.2.5 in Reference 2.2.24.

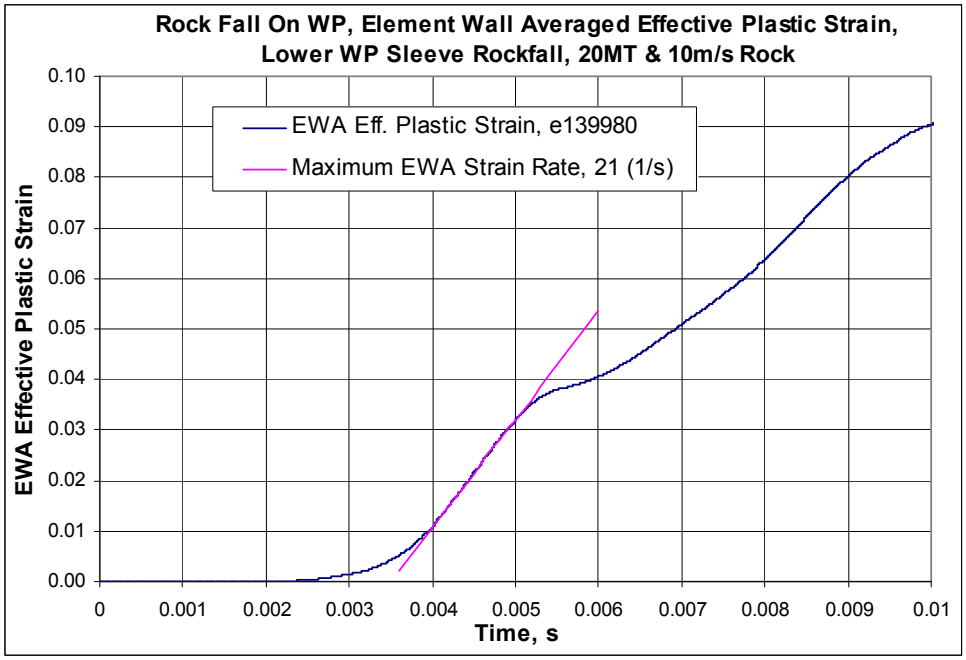

Figure 1. EWA Effective Plastic Strain Rock-WP Impact on Lower Sleeve

3.2.4 Poisson's Ratio of Alloy 22

The room temperature Poisson's ratio of Alloy 22 is not published in traditional sources. Therefore, the room temperature Poisson's ratio of Alloy 625 (SB-443 N06625) is assumed for Alloy 22. The impact of this assumption is anticipated to be negligible.

Rationale– The chemical compositions of Alloy 22 and Alloy 625 are similar since they are both 600 Series nickel-base alloys (Ref. 2.2.3 [Section II, Part B, SB-575, Table 1] and Ref. 2.2.2 [p. 143], respectively). Therefore, the difference in their Poisson's ratio is expected to be small. Furthermore, there are only small differences in RT Poisson's ratio values for the family of 600 Series nickel-based alloys:

Alloy 600 [UNS N06600] = 0.290 (Ref. 2.2.2, p.141)
Alloy 625 [UNS N06625] = 0.278 (Ref. 2.2.2, p.143)
Alloy 690 [UNS N06690] = 0.289 (Ref. 2.2.2, p.145)

The impact on stress results of small differences in Poisson's ratio is anticipated to be negligible. Stress formulas for cylindrical shells (Ref. 2.2.54, Table 30) indicate insensitivity to Poisson's ratio. For the loading case of uniform radial shear loads, the maximum hoop circumferential membrane stress, the key breaching stress, is proportional to Poisson's ratio, υ, through the term $(1-\upsilon^2)^{1/4}$. Using the lowest and highest υ values of the three 600 Series nickel-base alloys, 0.278 and 0.290, the difference in maximum hoop circumferential membrane stress values is a negligible 0.2%. Therefore, the study of parametric variations provides verification of this assumption per Reference 2.1.1 page 4 ("*Verification may include . . . studies of parametric*

variations") and further verification of this assumption is not required. This assumption is used in Section 6.1 and corresponds to Section 5.2.8.2 in Reference 2.2.24.

3.2.5 Poisson's Ratio of 316L Stainless Steel

The room temperature Poisson's ratio of 316L SS is not published in traditional sources. Therefore the room temperature Poisson's ratio of 316 SS is assumed for 316L SS. The impact of this assumption is anticipated to be negligible.

Rationale– The chemical compositions of 316L SS and 316 SS are similar (see Ref. 2.2.3, Section II, Part A, SA-240, Table 1) because they are both 300 Series (austenitic) stainless steels. Therefore the differences in their Poisson's ratio values are expected to be small. The 300 Series stainless steels have a relatively small range of RT Poisson ratio values:

Type 304 SS [UNS S304000] = 0.290 (Ref. 2.2.2, p. 755, Figure 15)
Type 316 SS [UNS S316000] = 0.298 (Ref. 2.2.2, p. 755, Figure 15)
Type 310 SS [UNS S310000] = 0.308 (Ref. 2.2.2, p. 755, Figure 15)

The impact on stress results of small differences in Poisson's ratio is anticipated to be negligible. Stress formulas for cylindrical shells (Ref. 2.2.54, Table 30) indicate insensitivity to Poisson's ratio. For the loading case of uniform radial shear loads, the maximum hoop circumferential membrane stress, the key breaching stress, is proportional to Poisson's ratio, υ, through the term $(1-\upsilon^2)^{1/4}$. Using the lowest and highest υ values of the three 300 Series stainless steels, 0.290 and 0.308, the difference in maximum hoop circumferential membrane stress values is a negligible 0.3%. Therefore, the study of parametric variations provides verification of this assumption per Reference 2.1.1 page 4 ("*Verification may include . . . studies of parametric variations*") and further verification of this assumption is not required. This assumption is used in Section 6.1 and corresponds to Section 5.2.8.4 in Reference 2.2.24.

3.2.6 Corrosion of Alloy 22

Unless noted otherwise, an upper bound value of the general corrosion rate for Alloy 22, 256 nm/year (0.0000101 in./yr) (Ref. 2.2.25, "Model Analysis Summary I", 99.99th percentile rate at 150°C), is assumed in these calculations. This corrosion assumption provides a consistent comparison with earlier rock fall calculations. This general corrosion is modeled by reducing the thickness of the WP OCB, WP sleeves, and the WP lids by 2.56 mm (0.101 in.), which is equivalent to the upper bound of the general corrosion rate over the regulatory period of 10,000 yrs. The EP plate corrosion has no significant effect on these comparisons. Therefore, the initial material thicknesses are used for the emplacement pallet components.

Rationale– This assumption thins the components of the WP under investigation so the reported stress intensities are slightly higher (conservative) than for the uncorroded condition. Once the worst case orientation is identified with the use of models that include the corrosion condition, the uncorroded case is run for that orientation. The effect of corrosion on identifying the orientation of the worst case scenario is insignificant. Therefore this assumption does not require verification. This assumption is used in Section 6.3.

3.2.7 The Uniform Strain of 316L Stainless Steel

The RT uniform strain (strain corresponding to tensile strength) of 316L SS is not listed in traditional sources. Therefore, it is assumed that the RT uniform strain is 60% of the RT minimum specified elongation (strain corresponding to rupture point in tensile test).

Rationale– The shape of the stress-strain curve for 316L SS that leads to the 60% selection is based on testing of "as-received" 316L SS material at a moderate strain rate, 8 s^{-1} (see Ref. 2.2.6, p. 305). Therefore this assumption does not require verification. This assumption is used in Section 6.1.2 and corresponds to Section 5.2.6.2 in Reference 2.2.24.

3.2.8 The Uniform Strain of Alloy 22

The RT uniform strain of Alloy 22 is not listed in traditional sources. Therefore, it is assumed that the RT uniform strain is 90% of the RT minimum specified elongation for Alloy 22.

Rationale– The rationale for this assumption is based on measurements of RT engineering stress-strain curves for Alloy 22 (DTN: LL020603612251.015, Ref. 2.2.7). The use of Reference 2.2.7 was approved as the appropriate data for the intended use in an Information Exchange Document (Ref. 2.2.56). Therefore this assumption does not require verification. This assumption is used in Section 6.1.2 and corresponds to Section 5.2.6.3 in Reference 2.2.24.

3.2.9 The Uniform Strain of 316 Stainless Steel

The uniform strain of 316 SS is not listed in traditional sources. Therefore, it is assumed that the RT uniform strain is 90% of the RT minimum specified elongation.

Rationale– The rationale for this assumption is the shape of the stress-strain curve for 316 SS from a qualified source (Ref. 2.2.6, p. 304). Therefore this assumption does not require verification. This assumption is used in Section 6.1.2 and corresponds to Section 5.2.6.3 in Reference 2.2.24.

3.2.10 Friction Coefficient between 316 and 316L Stainless Steel

The friction coefficient for contacts occurring between the 316 SS and 316L SS is not available in traditional sources. It is, therefore, assumed that the dynamic (sliding) friction coefficient for this contact is 0.4.

Rationale– The rationale for this assumption is that this friction coefficient represents the lower (conservative – less energy lost due to WP internal component contact) bound for the steel-on-steel contacts (Ref. 2.2.9, Table 3.2.1, p. 3-26 and Ref. 2.2.10, p. 441). Therefore this assumption does not require verification. This assumption is used in Section 6.5.

3.2.11 Friction Coefficient between Alloy 22 and Other Metallic Materials

The friction coefficients for contacts among the Alloy 22 components, or the contacts involving Alloy 22 and 316 SS, are not available in traditional sources. It is, therefore, assumed that the dynamic (sliding) friction coefficient for both of these contacts is 0.4.

Rationale– This friction coefficient represents the lower (conservative – less energy lost due to WP internal component contact) bound for most dry nickel-on-steel and nickel-on-nickel contacts (Ref. 2.2.9, Table 3.2.1, p. 3-26); nickel being the dominant component in Alloy 22 (Ref. 2.2.3, Section II, Part B, SB-575, Table 1). Therefore this assumption does not require verification. This assumption is used in Section 6.5 and corresponds to Section 5.2.14.1 in Reference 2.2.24.

3.2.12 Friction Coefficient between Metal and Rock

The friction coefficient for contacts occurring between the rock and Alloy 22 (OCB) or rock and 316 SS (Rockbolt) is not available in traditional sources. It is, therefore, assumed that the dynamic (sliding) friction coefficient for this contact is 0.525.

Rationale– For an estimate of the dynamic metal-on-stone friction coefficient values it is recommended (Ref. 2.2.11, p. 306) that the static metal-on-stone friction values be reduced by 25%. Reducing the upper bound static metal-on-stone friction value in Reference 2.2.11 (Table 8.1, p. 306) by 25% leads to 0.525. This estimated dynamic friction value represents the upper (conservative – less rock spread and rockbolt slip) end of the range of dynamic friction and therefore does not require verification. This assumption is used in Section 6.5.

3.2.13 Variation of Functional Friction Coefficients

The variation of functional friction coefficient between the static and dynamic value as a function of relative velocity of the surfaces in contact is not available in traditional sources for the materials used in this calculation. Therefore, the effect of relative velocity of the surfaces in contact is neglected in these calculations by assuming that the functional friction coefficients and static friction coefficients are both equal to the dynamic friction coefficient. The impact of this assumption on results presented in this document is anticipated to be negligible.

Rationale– This assumption provides a conservative bounding set of results by minimizing the friction coefficient within the given finite element analysis framework (the lone exception being the use of the upper bound of the estimated dynamic friction between metal and rock as discussed in Assumption 3.2.12). Therefore this assumption does not require verification. This assumption is used in Section 6.5 and corresponds to Section 5.2.14.2 in Reference 2.2.24.

3.2.14 Rock Shape

The rock shape is assumed to be a rectangular prism.

Rationale– The rock block data shows that some of the rock blocks are essentially rectangular prisms. A finite element representation (FER) of the rock with an inclined rectangular prism provides a conservative approach from the point of view that the rock center of gravity is located directly above the point of impact, transferring the maximum linear momentum to the WP. Therefore this assumption does not require verification. The sharp edge of the prism also results in maximum stresses in the WP. Section 5.3 of Reference 2.2.12 documents the calculations of the vertex coordinates of the prism in order to calculate the enveloping dimensions. This assumption is used in Section 6.5 and is consistent with Section 5.2.16.6 in Reference 2.2.24.

3.2.15 Bounding Credible Rock Fall

Bounding characteristics of a credible rock fall expected in an emplacement drift located in a nonlithophysal rock unit during the preclosure period is assumed in subsequent calculations. These characteristics are summarized in Table 1 (Ref. 2.2.28, Section 6.4.5.2 and 6.4.6).

Table 1. Bounding Characteristics of Credible Rock Falls

Type of rock fall	Maximum kinetic energy at impact	Maximum velocity at impact	Maximum mass
Single rock fall	$1.0 * 10^6$ J ($737,560$ ft·lb$_f$)	10 m/s (32.8 ft/s)	20.0 MT (44,092 lbs)
Two rock falls, same location – Total for both rocks	$1.0 * 10^6$ J (737,560 ft·lb$_f$)	9.96 m/s (32.7 ft/s) & 6.0 m/s (19.7 ft/s)	20.0 MT (44,092 lbs) & 0.50 MT (1,102 lbs)
Multiple rock falls, same location – Total for Five rocks tied by Rockbolt [a]	$2.0 * 10^4$ J ($14,751$ ft·lb$_f$)	4.3 m/s (14.1 ft/s)	2.15 MT (4,740 lbs)

MT: metric tons.
J: Joules.
[a] Maximum kinetic energy for multiple rock fall scenario recommended (Reference 2.2.28, Section 6.4.6) to be conservatively bounded with a total kinetic energy of $1.5 * 10^4$ J, with an impact velocity of 3.74 m/s.

These rock blocks are assumed to represent bounding rock kinetic energy, mass, and velocities that may occur during the pre-closure period.

Rationale– A probabilistic characterization of preclosure rock falls in emplacement drifts was performed that bounded the credible rock fall scenarios (Ref. 2.2.28, Sections 6.4.5.2.5 and 7). Therefore this assumption does not require verification. This assumption is used in Section 6.5.

3.2.16 Geometric Simplification of the PWR Waste Form Discretization

The exact geometries of the commercial waste forms (PWR fuel assemblies) are simplified for the purpose of this calculation in such a way that their total mass is assumed to be distributed within a bar of square cross section with uniform density. The following design parameters are assumed for the PWR spent nuclear fuel assemblies to be loaded into a TAD bearing WP loaded in a 21-PWR configuration: mass = 762 kg (1,680 lbs), length = 4.407 m (173.5 in.), width = 0.217 m (8.54 in.).

Rationale– The rationale for this assumption is that a simplified FER is used without affecting the computational results. The length and weight parameters correspond to the B&W 15x15 fuel assembly, which is the heaviest PWR fuel assembly (Ref. 2.2.18, Table 8). Therefore this assumption does not require verification. This assumption is used in Section 6.5 (Case #6a) and corresponds to Section 5.2.9.1 in Reference 2.2.24.

3.2.17 Material Simplification of the PWR Waste Form Properties

The commercial waste forms (PWR fuel assemblies) are assumed to be made of 304 SS.

Rationale– Because the end fittings of the waste forms are made of 304 SS (collaborated by Reference 2.2.15, Sections 2.1.2.2 and 2.1.2.5, Table 2.1), and they are the parts that will come

in contact with other components. This assumption is used in Sections 6.1 and 6.5 and corresponds to Section 5.2.9.2 in Reference 2.2.24.

3.2.18 Compressive Strength of Rock

A recommended value of the nonlithophysal rock block compressive strength, 70 MPa (10 ksi), is provided in Reference 2.2.17, Figure 1. Therefore, for the purpose of the present calculation, the compressive strength of the rock blocks is assumed to be 70 MPa (10 ksi).

Rationale– This assumption is based on the recommended compressive strength value for nonlithophysal rock blocks of significant size (3000 mm (118 in.) and larger, Ref. 2.2.17, Figure 1). The compressive strength value is the stress point in the rock after which the constitutive behavior of the rock is assumed to be ideally perfectly plastic with constant stress as strain increases. This assumption is used in Sections 6.1.

3.2.19 Poisson Ratio and Modulus of Elasticity of Rock

The mean values of the modulus of elasticity and Poisson's ratio of the TSw2 rock are given in Reference 2.2.17, Table 2. For the purpose of the present calculation, the mean values of modulus of elasticity, 33.6 GPa ($4.87*10^6$ psi), and Poisson's ratio, 0.20, are used.

Rationale– The mean values for Poisson's ratio and modulus of elasticity agree well with typical values of said properties for the nonlithophysal rocks in which some of the emplacement drifts are expected to be placed. Therefore this assumption will have negligible effect on the calculation results and does not require verification. This assumption is used in Section 6.1.

3.2.20 Rock Density

The density of the TSw2 rock is assumed to be 2411 kg/m^3 (0.0871 lb/in^3).

Rationale– The density value is the mean density value of all Topopah Spring Welded rocks in Reference 2.2.17, Table 1. It should be noted though that this assumption has no significant effect on the calculation results since the important input parameter is the mass of the rock regardless of the density. Therefore this assumption does not require verification. The rock shape is discussed in Assumption 3.2.14. Small adjustments to the density are made in the LS-DYNA input to provide an accurate rock mass. This assumption is used in Sections 6.1 and 6.5.

3.2.21 Poisson's Ratio for 304L Stainless Steel

Poisson's ratio for 304L SS is not published in traditional sources. Therefore, it is assumed to be the same as Poisson's ratio for 304 SS (Ref. 2.2.2, Figure 15, p. 755).

Rationale– The rationale for this assumption is that the chemical compositions of 304L stainless steel and 304 stainless steel are similar (Ref. 2.2.3, Section II, Part A, SA-240, Table 1) because they are both 300 Series (austenitic) stainless steels. Therefore the differences in their Poisson's ratio values are expected to be small. The 300 Series stainless steels have a relatively small range of RT Poisson ratio values:

Type 304 SS [UNS S304000] = 0.290 (Ref. 2.2.2, p. 755, Figure 15)
Type 316 SS [UNS S316000] = 0.298 (Ref. 2.2.2, p. 755, Figure 15)
Type 310 SS [UNS S310000] = 0.308 (Ref. 2.2.2, p. 755, Figure 15)

The impact on stress results of small differences in Poisson's ratio is anticipated to be negligible. Stress formulas for cylindrical shells (Ref. 2.2.54, Table 30) indicate insensitivity to Poisson's ratio. For the loading case of uniform radial shear loads, the maximum hoop circumferential membrane stress, the key breaching stress, is proportional to Poisson's ratio, υ, through the term $(1-\upsilon^2)^{1/4}$. Using the lowest and highest υ values of the three 300 Series stainless steels, 0.290 and 0.308, the difference in maximum hoop circumferential membrane stress values is a negligible 0.3%. Therefore, the study of parametric variations provides verification of this assumption per Reference 2.1.1 page 4 ("*Verification may include . . . studies of parametric variations*") and further verification of this assumption is not required. This assumption is used in Section 6.1 and corresponds to Section 5.2.8.5 in Reference 2.2.24.

3.2.22 Uniform Strain of A 516 Carbon Steel

The uniform strain of A 516 CS is not published in traditional sources. Therefore, it is conservatively assumed that the uniform strain is 50 percent of the elongation.

Rationale– The rationale for this assumption is the nature of the stress-strain curve for A 36 CS (Ref. 2.2.6, p. 186), which has a similar chemical composition as A 516 CS (Ref. 2.2.3, Section II, Part A, SA-516/SA-516M, Table 1 and SA-36/SA-36M, Table 2). Use of this assumption is limited to the waste form basket structure whose behavior will have an insignificant effect on the OCB structural response. Therefore this assumption does not require verification. This assumption is used in Section 6.1.2 and corresponds to Section 5.2.6.1 in Reference 2.2.24.

3.2.23 Strain Rate Dependent Properties of Rock

The strain rate-dependent properties of the TSw2 rock block are not published in traditional sources. The properties obtained under the static loading conditions are assumed for the rock block. The impact of using properties obtained under static loading conditions is anticipated to be small.

Rationale– The rationale for this assumption is that "the properties of most rocks can be regarded as being virtually independent of strain rate in the range covered by the usual laboratory tests" (Ref. 2.2.20, p. 144) and that the strain rates in the rock are low at the time of maximum stress in the outer shell. Therefore this assumption does not require verification. This assumption is used in Section 6.1.

3.2.24 Simplification of Loaded Internals of the WP

The geometries of the loaded PWR waste form and 21-PWR basket internals of the waste packages are simplified for the purpose of efficient structural calculations. For all TAD bearing WP cases except Case #6a, the TAD canistered SNF are developed as thick shell cylinders in the TAD canister with the appropriate mass values to account for the waste forms that are not explicitly modeled. The maximum recordable weight, 49,320 kilogram (54 ton), is assumed to

be distributed evenly in a thick-walled (9.1 inch (23 cm) – see Section 6.2.1) cylinder with a 15 inch (38 cm) top plug and 3.5 inch (8.9 cm) bottom lid (Ref. 2.2.26, Figure C-17, Note 3) and properties of 316L SS (Ref. 2.2.26, Figure C-17, Note 1). Additionally, the overall center of gravity of the total mass of the canister is located 110.6 inches (2.81 m) from the bottom external surface and satisfies the Reference 2.2.26, Figure C-17 specification to be between 103 and 123 inches (2.62 and 3.12 m).

For rock fall on the middle of the TAD bearing waste package the wall of the TAD canister was represented with a 1 inch (2.54 cm) thickness and the total mass of the TAD canister was maintained by modeling a mass balancing cylinder inside the TAD cavity. An additional case (Case #6a) includes a 21-PWR configuration within the TAD canister to include the restraint of the canistered waste form basket structure as the rock strike pushes into the canister wall. The 21-PWR (Case #6a) and 5-DHLW/DOE Codisposal (Cases #15 and #16) structural internals (i.e. baskets and divider plates) use configurations and materials that are consistent with References 2.2.58 to 2.2.60 and References 2.2.47 to 2.2.49, respectively. Note the material used to model in the 21-PWR basket (A 516 CS) has been superseded by the material specified (300 Series SS) in the *Transportation, Aging and Disposal Canister System Performance Specification* (Reference 2.2.61, Section 3.1.8). Case #6a, where the 21-PWR basket structure is explicitly modeled using A 516 CS, does not require an updated simulation because the purpose of that sensitivity case was only to show that conservative (higher) OCB stress intensities are calculated without the presence of structural internal components in the TAD canister.

Rationale– The rationale for modeling the TAD canister as a thick shelled cylinder is that it simplifies the FER while preserving the mass effects that a fully loaded canister could impart on the OCB structural response to rock fall. Note that the use of information from Reference 2.2.26, Figure C-17 is suitable since the reference document has been established as a requirement (Reference 2.2.16, Section 12.2.1.2). In Case #6a, where the structural internals (i.e. basket) are explicitly modeled, the internal components of the TAD canister provide restraints that reduce the stress intensities in the OCB from the higher levels calculated using a TAD canister without internal components (Case #6). Therefore, regardless of the material used to model the structural internals, the rock fall on the middle of the WP case where there are no structural internal components modeled in the TAD canister (Case #6) will respond with a more conservative (higher) stress intensity in the OCB than the case where canister internals are included in the model (Case #6a). This assumption is used in Sections 6.1 and 6.2.

3.2.25 The Uniform Strain of 304 Stainless Steel

The uniform strain of 304 SS is not listed in traditional sources. Therefore, it is assumed that the uniform strain is 75% of the minimum specified elongation.

Rationale– The rationale for this assumption is the shape of the stress-strain curve for 304 SS from a qualified source (Ref. 2.2.6, p. 294). Therefore this assumption does not require verification. This assumption is used in Section 6.1.2 and corresponds to Section 5.2.6.4 in Reference 2.2.24.

3.2.26 The Uniform Strain of 304L Stainless Steel

The uniform strain of 304L SS is not listed in traditional sources. Therefore, it is assumed that the uniform strain is 75% of the minimum specified elongation.

Rationale– The rationale for this assumption is the shape of the stress-strain curve for 304 SS (Ref. 2.2.6, p. 294), which has a similar chemical composition to 304L SS (Ref. 2.2.3, Section II, Part A, SA-240, Table 1). Use of this assumption is limited to the HLW canister conceptualization in the Co-disposal WP whose behavior will have an insignificant effect on the OCB structural response. Therefore this assumption does not require verification. This assumption is used in Section 6.1.2.

4. METHODOLOGY

4.1 QUALITY ASSURANCE

This calculation was prepared in accordance with EG-PRO-3DP-G04B-00037, *Calculation and Analyses* (Ref. 2.1.1). The Waste Package is classified as a Safety Category item (important to safety and important to waste isolation) on the Q-List (Ref. 2.2.22, Table A-1, pages A-4 and A-9). Therefore, this document is subject to the requirements of the BSC Quality Management Directive (Ref. 2.2.55, Sections 2.1.C.1.1.a.i and 17.E) and the approved version is designated as QA: QA.

4.2 USE OF SOFTWARE

The computer code used for dynamic structural analysis in this calculation is the commercially available LS-DYNA V.970.3858 D MPP (Software Tracking Number [STN]: 10300-970.3858 D MPP-00, Ref. 2.2.23) finite element analysis package. LS-DYNA is obtained from Software Configuration Management in accordance with appropriate procedures. This version of the LS-DYNA code is also identified by the software tracking number (STN): 10300-970.3858 D MPP-00 (Ref. 2.2.23) and has an available validation test report (Ref. 2.2.27). LS-DYNA is a commercially available FEA code and is appropriate for the WP structural analyses performed in this calculation. The simulations were all performed with LS-DYNA V.970.3858 D MPP on a Hewlett-Packard (HP) Itanium2 platform cluster which uses the HP-UX 11.22 operating system. The HP Itanium2 platform computer cluster is identified with one tag number: 501711. All workstations are located in Las Vegas, Nevada. The LS-DYNA evaluation performed for this calculation is fully within the range of the validation (Ref. 2.2.27) performed for the LS-DYNA code. Access to the code is granted by Software Configuration Management in accordance with the appropriate procedures. LS-DYNA is listed in the *Repository Project Management Automation Plan* (Reference 2.1.3, Table 6-1). The results of this calculation are provided in terms of stress intensities.

The finite element mesh, which is subsequently used in the LS-DYNA solver, is developed using TrueGrid Version 2.2 (hereinafter referred to as "TrueGrid"). TrueGrid is a pre-processing tool for graphical and geometrical representation and therefore is Level 2 software as defined in *Software Management* (Ref. 2.1.2, Section 4 and Attachment 12). The meshing is executed on an HP 9000 series UNIX workstation (Operating System HP-UX 11.0), identified with Yucca Mountain Project tag number 151324, and located in Las Vegas, Nevada. The suitability and adequacy of the mesh generated using TrueGrid is based on visual examination, engineering

judgment, and the results of the mesh verification exercise performed in section 7.1. TrueGrid is listed in the *Repository Project Management Automation Plan* (Reference 2.1.3, Table 6-1).

LS-PREPOST V1.0 (Livermore Software Technology Corporation) is the postprocessor used only for visual display and graphical representation of LS-DYNA FERs and results and therefore is Level 2 software as defined in Reference 2.1.2, Attachment 12. The suitability and adequacy of the displayed results is based on visual examination and engineering judgment. The post processing is performed on HP Itanium2 (IA64) series UNIX workstations (Operating System HP-UX 11.22), collectively identified with the Yucca Mountain Project tag number 501711, and located in Las Vegas, Nevada.

The commercially available Microsoft Office Excel 2003 (11.8105.8107 SP2) spreadsheet code, which is a component of Microsoft Office 2003 Professional, is used to perform simple data conversion (maximum shear stress to stress intensity) and plotting. These results were verified by checks using hand calculations and plots were verified by visual inspection. Usage of Microsoft Office 2003 Professional in this calculation constitutes Level 2 software usage, as defined in IT-PRO-0011 (Reference 2.1.2, Section 4 and Attachment 12). Microsoft Office 2003 Professional is listed in the current controlled Software Report, as well as the Repository Project Management Automation Plan (Reference 2.1.3, Table 6-1). Microsoft Office Excel 2003 was executed on a PC with X86 architecture running the Microsoft Windows XP Professional operating system, Version 5.1.2600, Service Pack 2, Build 2600.

4.3 APPROACH

This is a summary description of the methodology used to conduct this calculation.

1. Using the TrueGrid software package, discretize a "keyword" finite element mesh representation of a TAD bearing WP. Hand calculations are performed to calculate the wall thickness of the simplified loaded TAD canister (see Assumption 3.2.24 and Section 6.2.1) and to size the 20 metric tons (MT) (44,092 lbs) rock (see Section 6.4).

2. Set up LS-DYNA input deck to simulate the WP being struck by an emplacement drift rock fall (Nonlithophysal zone) scenario. Selection of material properties and rock fall scenario parameters are described in the *Waste Package Component Design Methodology Report* (Ref. 2.2.24, Sections 5.2.16 and 6.2.2.4). The bounding credible single rock fall during the preclosure period is 20 MT (44,092 lbs) with a velocity at impact on the WP of 10 m/s (32.8 ft/s) (Ref. 2.2.28, Section 7). The bounding credible multiple rock fall during preclosure includes a 20 MT (44,092 lbs) rock followed by an average expected size rock, the kinetic energy of both rocks summing to 1,000,000 J (737,560 $ft \cdot lb_f$) (Ref. 2.2.28, Section 6.4.5.2). For the elevated temperature material properties used in the LS-DYNA input deck, hand calculations are performed to interpolate material properties from available data, See Section 6.1. Hand calculations are also performed to derive the Tangent Moduli of the materials used in the LS-DYNA models, See Section 6.1.3.

3. Verify the level of mesh discretization that is adequate for this analysis using the mesh optimization technique described in the *Waste Package Component Design Methodology Report* (Ref 2.2.24, Section 6.2.3).

4. Simulate rock fall impacts on four locations that will capture the maximum stress intensities that could be generated in the OCB due to preclosure rock fall. The impact locations considered are: the upper WP sleeve, a point near the quarter point along the WP length, a point at the middle of the WP length, and the lower WP sleeve. Modify each FER so that the level of mesh discretization is adequate at each of the impact locations.

5. Use a bounding credible single rock, both with and without a rockbolt, and the bounding credible impact velocity to determine the maximum OCB primary membrane stress intensities.

6. Using the impact location that produced the highest primary membrane stress intensities in the OCB, run simulations analyzing the primary membrane stress intensities generated in the OCB of a 5DHLW/DOE SNF Co-disposal short WP.

7. Using the impact location that produced the highest primary membrane stress intensities in the OCB, run simulations analyzing the primary membrane stress intensities generated in the OCB of a TAD bearing WP due to multiple rock impact scenarios (Ref. 2.2.28, Section 6.4.5.2.4) .

5. LIST OF ATTACHMENTS

		Number of Pages
Attachment I.	Directory Listing of (Data DVD) Electronic Files	2
Attachment II.	Figures obtained from LS-DYNA	3
Attachment III.	Data DVD Attachment	Electronic file, 1 disk

6. BODY OF CALCULATION

6.1 MATERIAL PROPERTIES

Room temperature (RT) material properties obtained under static loading conditions are used for Alloy 22, 316 SS, and 316L SS (see Assumptions 3.1.1, 3.2.1 and 3.2.3). Also, RT material properties obtained under static loading conditions are used for TSw2 rock (see Assumptions 3.2.2 and 3.2.23). When elevated temperature data is available, the material properties are obtained by linear interpolation of the bounding temperature properties using the formula:

$$p = p\ T\ = p_l + \left(\frac{T - T_l}{T_u - T_l} \right) \cdot \left(p_u - p_l \right) \qquad \text{Equation 6.1}$$

Where subscripts *u* and *l* denote the upper and lower bounding values of generic material property *p* at the corresponding bounding temperatures *T*.

Stress units are Pascal (*Pa*), Mega Pascal ($MPa = 10^6\ Pa$), Giga Pascal ($GPa = 10^9\ Pa$), lb/in^2 (*psi*) and $ksi = 10^3\ psi$.

6.1.1 Listing of Material Properties

Unless noted, the material properties listed in this section are at room temperature.

SB-575 UNS N06022 (Alloy 22 used in OCB, WP Sleeves, and Pallet Base):

Density = 8690 kg/m^3 (0.314 lb/in^3) (Ref. 2.2.3, Section II, Part B, SB-575, Section 7.1)

Yield strength = 310 MPa (45.0 ksi) (Ref. 2.2.3, Section II, Part D, Subpart 1, Table Y-1)

Tensile strength = 689 MPa (100 ksi) (Ref. 2.2.3, Section II, Part D, Subpart 1, Table U)

Elongation = 0.45 (Ref. 2.2.3, Section II, Part B, SB-575, Table 4)

Poisson's ratio = 0.278 (Assumption 3.2.4)

Modulus of elasticity = 206 GPa (29.9 * 10^6 psi) (Ref. 2.2.8, p. 14, vendor supplied data suitable for the intended use)

SA-240 UNS S31600 (316 SS used in Inner Vessel, Pallet Longitudinal Posts and Rockbolts):

Density = 7980 kg/m^3 (0.288 lb/in^3) (Ref. 2.2.4, Table X1.1, p. 7)

Yield strength = 207 MPa (30.0 ksi) (Ref. 2.2.3, Section II, Part D, Subpart 1, Table Y-1)

Tensile strength = 517 MPa (75.0 ksi) (Ref. 2.2.3, Section II, Part D, Subpart 1, Table U)

Elongation = 0.40 (Ref. 2.2.3, Section II, Part A, SA-240, Table 2)

Poisson's ratio = 0.298 (Ref. 2.2.2, Figure 15, p. 755)

Modulus of elasticity = 195 GPa (28.3 *10^6 psi) (Ref. 2.2.3, Section II, Part D, Subpart 2, Table TM-1)

SA-240 UNS S31603 (316L SS used in TAD Canister (Assumption 3.1.2) and the DOE SNF Canister in the Co-Disposal WP (Ref. 2.2.16, Section 11.2.2.8)):

Density = 7980 kg/m^3 (0.288 lb/in^3) (Ref. 2.2.4, Table X1.1, p. 7)

Yield strength = 172 MPa (25.0 ksi) (Ref. 2.2.3, Section II, Part D, Subpart 1, Table Y-1)

Tensile strength = 483 MPa (70.0 ksi) (Ref. 2.2.3, Section II, Part D, Subpart 1, Table U)

Elongation = 0.40 (Ref. 2.2.3, Section II, Part A, SA-240, Table 2)

Poisson's ratio = 0.298 (see Assumption 3.2.5)

Modulus of elasticity = 195 GPa (28.3 *10^6 psi) (Ref. 2.2.3, Section II, Part D, Subpart 2, Table TM-1)

SA-240 UNS S30400 (304 SS used in 21-PWR Fuel Assembly) (Assumption 3.2.17):

Yield strength = 207 MPa (30 ksi) (Ref. 2.2.3, Section II, Part D, Subpart 1, Table Y-1)

Tensile strength = 517 MPa (75 ksi) (Ref. 2.2.3, Section II, Part D, Subpart 1, Table U)

Elongation = 0.40 (Ref. 2.2.3, Section II, Part A, SA-240, Table 2)

Poisson's ratio = 0.29 (Ref. 2.2.2, Figure 15, p. 755)

Modulus of elasticity = 195 GPa (28.3 *10^6 psi) (Ref. 2.2.3, Section II, Part D, Subpart 2, Table TM-1)

SA-516 UNS K02700 Grade 70 (A 516 Carbon Steel [CS] used in 21-PWR Fuel Basket, Assembly Tubes and Guides) (Assumption 3.2.24):

Density = 7850 kg/m^3 (0.284 lb/in^3) (Ref. 2.2.3, Section II, Part A, SA-20/SA20M, Section 14.1)

Yield strength = 262 MPa (38.0 ksi) (Ref. 2.2.3, Section II, Part D, Subpart 1, Table Y-1)

Tensile strength = 483 MPa (70 ksi) (Ref. 2.2.3, Section II, Part D, Subpart 1, Table U)

Elongation = 0.21 (Ref. 2.2.3, Section II, Part A, SA-516/SA-516M, Table 2)

Poisson's ratio = 0.3 (Ref. 2.2.19, p. 374)

Modulus of elasticity = 203 GPa (29.5 *10^6 psi) (Ref. 2.2.3, Section II, Part D, Subpart 2, Table TM-1)

SA-516 UNS K02700 Grade 70 (at 350 °C (662 °F), A 516 Carbon Steel [CS] used in Co-Disposal WP Basket Divider Plates):

Density = 7850 kg/m^3 (0.284 lb/in^3) (Ref. 2.2.3, Section II, Part A, SA-20/SA20M, Section 14.1)

Yield strength = 194 MPa (28.2 ksi) (at 343 °C (650 °F) Ref. 2.2.3, Section II, Part D, Subpart 1, Table Y-1)

Yield strength = 188 MPa (27.2 ksi) (at 371 °C (700 °F) Ref. 2.2.3, Section II, Part D, Subpart 1, Table Y-1)

Yield strength = 193 MPa (27.9 ksi) (Ref. 2.2.3, Section II, Part D, Subpart 1, Table Y-1, interpolate between 650 °F and 700 °F using Equation 6.1)

Tensile strength = 483 MPa (70 ksi) (Ref. 2.2.3, Section II, Part D, Subpart 1, Table U, constant between RT and 371 °C (700 °F))

Elongation = 0.21 (Ref. 2.2.3, Section II, Part A, SA-516/SA-516M, Table 2)

Poisson's ratio = 0.3 (Ref. 2.2.19, p. 374)

Modulus of elasticity = 184 GPa (26.7 *10^6 psi) (at 316 °C (600 °F) Ref. 2.2.3, Section II, Part D, Subpart 2, Table TM-1)
Modulus of elasticity = 176 GPa (25.5 *10^6 psi) (at 371 °C (700 °F) Ref. 2.2.3, Section II, Part D, Subpart 2, Table TM-1)
Modulus of elasticity = 179 GPa (26.0 *10^6 psi) (Ref. 2.2.3, Section II, Part D, Subpart 2, Table TM-1, interpolate between 600 °F and 700 °F using Equation 6.1)

SA-240 UNS S30403 (at 350 °C (662 °F), 304L SS used in the HLW Canister Conceptualization in the Co-Disposal WP):

Yield strength = 105 MPa (15.2 ksi) (at 343 °C (650 °F) Ref. 2.2.3, Section II, Part D, Subpart 1, Table Y-1)
Yield strength = 103 MPa (15.0 ksi) (at 371 °C (700 °F) Ref. 2.2.3, Section II, Part D, Subpart 1, Table Y-1)
Yield strength = 105 MPa (15.2 ksi) (Ref. 2.2.3, Section II, Part D, Subpart 1, Table Y-1, interpolate between 650 °F and 700 °F using Equation 6.1)

Tensile strength = 391 MPa (56.7 ksi) (at 343 °C (650 °F) Ref. 2.2.3, Section II, Part D, Subpart 1, Table U)
Tensile strength = 389 MPa (56.4 ksi) (at 371 °C (700 °F) Ref. 2.2.3, Section II, Part D, Subpart 1, Table U)
Tensile strength = 390 MPa (56.6 ksi) (Ref. 2.2.3, Section II, Part D, Subpart 1, Table U, interpolate between 650 °F and 700 °F using Equation 6.1)

Elongation = 0.40 (Ref. 2.2.3, Section II, Part A, SA-240, Table 2)

Poisson's ratio = 0.29 (Assumption 3.2.21)

Modulus of elasticity = 174 GPa (25.3 *10^6 psi) (at 316 °C (600 °F) Ref. 2.2.3, Section II, Part D, Subpart 2, Table TM-1)
Modulus of elasticity = 171 GPa (24.8 *10^6 psi) (at 371 °C (700 °F) Ref. 2.2.3, Section II, Part D, Subpart 2, Table TM-1)
Modulus of elasticity = 172 GPa (25.0 *10^6 psi) (Ref. 2.2.3, Section II, Part D, Subpart 2, Table TM-1, interpolate between 600 °F and 700 °F using Equation 6.1)

TSw2 Rock (used in all simulations):

Density = 2411 kg/m^3 (Assumption 3.2.20)

Poisson's ratio = 0.20 (Assumption 3.2.19)

Modulus of elasticity = 33.6 GPa (4.87*10^6 psi) (Assumption 3.2.19)

Unconfined compressive strength = 70 MPa (10 ksi) (Assumption 3.2.18)

6.1.2 Calculations for True Measures of Ductility

The material properties in Section 6.1.1 refer to engineering stress and strain definitions: $S = P / A_0$ and $e = (L - L_0) / L_0$ (see Ref. 2.2.1, Chapter 9). Where P stands for the force applied during a static tensile test, L is the length of the deformed specimen, and L_0 and A_0 are the original length and cross-sectional area of the specimen, respectively. The engineering stress-strain curve does not give a true indication of the deformation characteristics of a material during plastic deformation since it is based entirely on the original dimensions of the specimen. Hence, the constitutive relation in LS-DYNA is defined in terms of true stress and strain: $\sigma = P / A$ and $\varepsilon = \ln(L / L_0)$ where A is the deformed area (Ref. 2.2.1, Chapter 9).

The relationships between the true stress and strain definitions and the engineering stress and strain definitions, $\sigma = S(1 + e)$ and $\varepsilon = \ln(1 + e)$, can be readily derived based on constancy of volume ($A_0L_0 = AL$) and strain homogeneity during plastic deformation (Ref. 2.2.1, Chapter 9). These expressions are applicable only in the hardening region of the stress-strain curve that is limited by the onset of necking.

The following parameters are used in the subsequent calculations:
$S_y \cong \sigma_y$ = yield strength
S_u= engineering tensile strength
σ_u= true tensile strength
$e_y \cong \varepsilon_y$ = strain corresponding to yield strength
e_u = engineering strain corresponding to tensile strength (engineering uniform strain)
ε_u = true strain corresponding to tensile strength (true uniform strain)

In absence of data on the uniform strain in traditional sources, the uniform strain needs to be estimated based on the character of stress-strain curves and elongation (strain corresponding to rupture of the tensile specimen).

The stress-strain curves for Alloy 22 and 316 SS do not manifest significant three-stage (elastic-hardening-softening) deformation character (see Assumptions 3.2.8 and 3.2.9). Therefore, a reduction in elongation by 10% is assumed for the uniform strain.

For Alloy 22, the true measures of ductility at RT is calculated,
$e_u = 0.9 * \text{Elongation} = 0.9 * 0.45 = 0.41$
$\varepsilon_u = \ln (1 + e_u) = \ln (1 + 0.41) = 0.34$
$\sigma_u = S_u (1 + e_u) = 689 (1 + 0.41) = 971$ MPa (141 ksi)
Therefore, the true tensile strength of Alloy 22 at RT is 971 MPa (141 ksi).

For 316 SS, the true measures of ductility at RT is calculated,
$e_u = 0.9 * \text{Elongation} = 0.9 * 0.40 = 0.36$
$\varepsilon_u = \ln (1 + e_u) = \ln (1 + 0.36) = 0.31$
$\sigma_u = S_u (1 + e_u) = 517 (1 + 0.36) = 703$ MPa (102 ksi)
Therefore, the true tensile strength of 316 SS at RT is 703 MPa (102 ksi).

Unlike the previous two cases, the stress-strain curve for 316L SS exhibits pronounced three-stage (elastic-hardening-softening) deformation character. The uniform strain is, therefore, estimated to be 60% of elongation based on the available stress-strain curves (see Assumption 3.2.7).

For 316L SS, the true measures of ductility at RT is calculated,
e_u = 0.6 * Elongation = 0.6 * 0.40 = 0.24
$\varepsilon_u = \ln (1 + e_u) = \ln (1 + 0.24) = 0.22$
$\sigma_u = S_u (1 + e_u) = 483 (1 + 0.24) = 599$ MPa (86.9 ksi)
Therefore, the true tensile strength of 316L SS at RT is 599 MPa (86.9 ksi).

The stress-strain curve for A 516 CS is not available in traditional sources. The carbon structural steel, A 36 CS, has similar chemical contents with A 516 CS. Therefore, the stress-strain curve for A 36 CS is used to estimate the uniform strain (Assumption 3.2.22), which is determined to be 50% of elongation.
e_u = 0.5 * Elongation = 0.5 * 0.21 = 0.11
$\varepsilon_u = \ln (1 + e_u) = \ln (1 + 0.11) = 0.10$
$\sigma_u = S_u (1 + e_u) = 483 (1 + 0.11) = 536$ MPa (77.7 ksi)
Therefore, because the engineering tensile strength of 516 CS is the same at RT and 350 °C the true tensile strength of A 516 CS at both RT and 350 °C (662 °F) is 536 MPa (77.7 ksi).

For 304 SS, the stress-strain curve at RT indicates that the uniform strain is 0.30 (Assumption 3.2.25 and Ref. 2.2.6, page 294), which is 75% of the elongation value for 304 SS (0.40).
$\varepsilon_u = \ln (1 + e_u) = \ln (1 + 0.30) = 0.26$
$\sigma_u = S_u (1 + e_u) = 517 (1 + 0.30) = 672$ MPa (97.5 ksi)
Therefore, the true tensile strength of 304 SS at RT is 672 MPa (97.5 ksi).

For 304L SS, which has a similar chemical composition as 304 SS and the same RT elongation (Reference 2.2.3, Section II, Part A, SA-240, Table 2), a uniform strain value of 0.3 is used based on the stress-strain curve for 304 SS at RT (Ref. 2.2.6, page 294) (Assumption 3.2.26).
$\varepsilon_u = \ln (1 + e_u) = \ln (1 + 0.30) = 0.26$
$\sigma_u = S_u (1 + e_u) = 390 (1 + 0.30) = 507$ MPa (73.5 ksi)
Therefore, the true tensile strength of 304L SS at 350 °C (662 °F) is 507 MPa (73.5 ksi).

6.1.3 Calculations for Tangent Moduli

The results of this simulation are required to include elastic and plastic deformations for all materials. When the materials are driven into the plastic range, the slope of the stress-strain curve continuously changes. A ductile failure is preceded by a protracted regime of hardening and substantial accumulation of inelastic strains. Thus, a simplification for the stress-strain curve is needed to incorporate plasticity into the FEA. A standard approximation commonly used in engineering is to use a straight line that connects the yield point and the tensile strength point of the material. The parameters used in the subsequent calculations in addition to those defined in Section 6.1.2 are modulus of elasticity (E) and tangent (hardening) modulus (E_1). The tangent modulus represents the slope of the stress-strain curve in the plastic region.

For Alloy 22 (used in OCB, WP Sleeves, and Pallet Base), the tangent modulus at RT is calculated using the true stress and strain values derived in Sections 6.1.1 and 6.1.2:
$E_1 = (\sigma_u - \sigma_y) / (\varepsilon_u - \sigma_y / E) = (0.971 - 0.310) / (0.34 - 0.310 / 206) = 1.95$ GPa (283 ksi)

For 316 SS (used in Inner Vessel and Pallet Longitudinal Posts) at RT:
$E_1 = (\sigma_u - \sigma_y) / (\varepsilon_u - \sigma_y / E) = (0.703 - 0.207) / (0.31 - 0.207 / 195) = 1.60$ GPa (232 ksi)

For 316L SS (used in TAD Canister and DOE SNF Canister in the Co-Disposal WP) at RT:
$E_1 = (\sigma_u - \sigma_y) / (\varepsilon_u - \sigma_y / E) = (0.599 - 0.172) / (0.22 - 0.172 / 195) = 1.95$ GPa (283 ksi)

For 304 SS (used in 21-PWR Fuel Assembly Conceptualization) at RT:
$E_1 = (\sigma_u - \sigma_y) / (\varepsilon_u - \sigma_y / E) = (0.672 - 0.207) / (0.26 - 0.207 / 195) = 1.80$ GPa (261 ksi)

For A516 CS (used in 21-PWR Fuel Basket Assembly Divider Plates) at RT:
$E_1 = (\sigma_u - \sigma_y) / (\varepsilon_u - \sigma_y / E) = (0.536 - 0.262) / (0.10 - 0.262 / 203) = 2.78$ GPa (403 ksi)

For A516 CS (used in Co-Disposal Basket Divider Plates) at 350 °C (662 °F):
$E_1 = (\sigma_u - \sigma_y) / (\varepsilon_u - \sigma_y / E) = (0.536 - 0.193) / (0.10 - 0.193 / 179) = 3.47$ GPa (503 ksi)

For 304L SS (used in HLW Canister Conceptualization in the Co-Disposal WP) at 350 °C:
$E_1 = (\sigma_u - \sigma_y) / (\varepsilon_u - \sigma_y / E) = (0.507 - 0.105) / (0.26 - 0.105 / 172) = 1.55$ GPa (225 ksi)

6.1.4 Constitutive Representation of Rock Behavior

In general, the constitutive representation of rock behavior (i.e., stress-strain relation) needs to address various complexities of rock deformation. In contrast to the elastic-ideally-brittle behavior of rock under tension, the stress-strain behavior of rock under compression can take numerous forms depending on the loading conditions (lateral confinement is a notable example), geometry (i.e., the slenderness ratio of the test specimen), and size. Brittle materials in general, when subjected to compression, exhibit a wide range of nonlinear stress-strain behaviors due to the nucleation, propagation, and coalescence of micro cracks under different boundary conditions (see Ref. 2.2.20, Sections 4.2 through 4.5). Moreover, the compressive strength of brittle materials (including rock) is significantly higher than their tensile strength. Finally, unlike engineering metals, the rocks may exhibit nonlinear behavior even under moderate hydrostatic compression, and there is a significant effect of size on strength (see Ref. 2.2.20; Sections 4, 6, and 7, for detailed discussion). A variety of constitutive representations have been developed to address the most prominent features of the behavior of brittle materials (for example, see Ref. 2.2.21, pages 362 and 363). These complex constitutive representations require a large number of input parameters. Some of these are not available at present for TSw2, while others are not intrinsic properties of rock but rather fitting parameters whose estimation requires test data currently unavailable for TSw2. Thus, a reasonable simplification of rock constitutive behavior is necessary. Fortunately, the stress state of the rocks is of no interest in this analysis and the rock deformation is important only in as much as it affects the stresses and strains in the waste package outer barrier, which is the objective of this calculation.

As a first approximation, the constitutive representation of rock behavior should appropriately capture local crushing of the rock at the point of impact, resulting in a reasonable distribution of

impact energy across the larger contact area. It is, therefore, considered appropriate to simplistically represent the rock behavior as elastic-ideally-plastic (Figure 2 and Ref. 2.2.20, Section 9). This representation of nonlinear behavior offers obvious advantages compared to the elastic representation for the given loading conditions. The unconfined compressive strength of rock, used as the yield strength in the constitutive representation, is one of the parameters in this study that affects the results. A conservative value of the unconfined compressive strength is, therefore, used to provide a bounding set of results. Having in mind that the loading conditions of the rock are predominantly compressive, 70 MPa is chosen as the representative upper bound rock strength (Assumption 3.2.18).

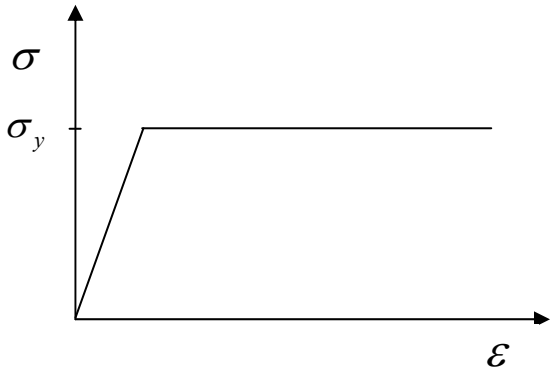

Figure 2. Elastic-Ideally-Plastic Constitutive Representation

6.2 MASS AND GEOMETRIC DIMENSIONS OF CANISTERED SPENT NUCLEAR FUELS

The following design parameters are used for the defense high-level radioactive waste (DHLW) canisters to be loaded into a 5-DHLW/DOE SNF Co-disposal Short waste package: mass = 2,500 kg (5512 lb), length = 3.0 m (118 in.), outside diameter = 0.61 m (24 in.), canister shell material is 304L stainless steel (Ref. 2.2.16, Section 11.2.2.7). In addition to these parameters: neck height = 0.21336 m (8.4 in.), neck diameter = 0.1684 m (6.63 in.) (Ref. 2.2.26, Figure C-20). Note that the use of information from Reference 2.2.26, Figure C-20 is suitable since this has been established as a requirement (Reference 2.2.16, Section 11.2.1.2)

The following design parameters are used for the DOE spent nuclear fuel (SNF) canisters (nominally 18 in x 10 ft (0.457 m x 3.048 m)) to be loaded into a 5-DHLW/DOE SNF Co-disposal Short waste package: mass = 2,270 kg (5004 lb), length = 3.0 m (118 in.), outside diameter = 0.4742 m (18.67 in.), canister shell material is 316L stainless steel (Ref. 2.2.16, Section 11.2.2.8).

For the TAD canister, this calculation is performed by using the bounding mass and geometric dimensions of the Naval SNF long canister (Assumption 3.1.2) obtained from Reference 2.2.26, Figure C-17: maximum recordable total mass = 49,320 kg (54.37 tons), maximum outside diameter = 1.689 m (66.5 in.), maximum length = 5.385 m (212 in.), canister shell material is

316L stainless steel (Assumption 3.1.2 and Reference 2.2.26, Figure C-17, Note 1). For the purposes of this calculation, the mass of the Naval SNF long canister is modeled as the maximum recordable total mass but the outside diameter is modeled as 1.679 m (66.12 in.), and the length is modeled as 5.350 m (210.63 in.). The internal structure of the WP is simplified in the FER by reducing the structure of the Naval SNF long canister to a thick walled (0.231 m (9.1 in.) – see Section 6.2.1) hollow cylinder with a 0.381 m (15 in.) top shield and 0.089 m (3.5 in.) bottom lid (Assumption 3.2.24). The density of 316L stainless steel is held constant as the cylinder wall thickness of the canister is back-calculated to closely match the maximum recordable mass of the Naval SNF long canister, See Section 6.2.1. Note that the overall center of gravity of the modeled canister is located 2.81 m (110.6 in.) from the canister's bottom external surface (see Section 6.2.2) which satisfies the requirement that the center of gravity be located between 2.62 m and 3.12 m (103 in. and 123 in.)(Reference 2.2.26, Figure C-17).

In the rock fall on mid package scenario and the rock fall on the quarter point of the package, the distortions caused by the rock will include a deflection in the side wall of the TAD canister. In order to capture more representative deflections of the TAD side wall, in the scenarios where that is possible, the thickness of the TAD canister's side walls is reduced to 0.0254 m (1 in.) thickness (Assumption 3.1.2) and the total mass of the TAD canister is maintained by modeling a mass-balancing cylinder of 316L stainless steel inside of the TAD cavity. The mass-balancing cylinder inside of the TAD canister is back calculated to maintain the same over-all mass of the canister.

6.2.1 Calculations for TAD Canister Wall Thickness

Total length of Canister = 210.63 in
= (210.63)/(12*3.281) m
= 5.3497 m

Top Lid (Plug) thickness = 15 in.
= (15)/(12*3.281) m
= 0.381 m

Bottom Lid thickness = 3.5 in.
= (3.5)/(12*3.281) m
= 0.0889 m

Canister outer diameter = 66.12 in.
= (66.12)/(12*3.281) m
= 1.6794 m

Canister Shell length = (210.63) – (15 + 3.5) in.
= 192.13 in.
= (192.13)/(12*3.281) m
= 4.88 m

Canister weight = 49.32 Metric Ton
= 49,320 kg

= (49,320*2.2046) lb
= 108,731 lb
= (108,731/2000) = 54.37 Ton (Eng.)

Canister material (316L SS) density = 7980 kg/m^3

Top Lid (Plug) weight = $(\pi/4)*(dia^2)*(length)*density$
= $(\pi/4)*(1.6794^2)*(0.381)*(7980)$ kg
= 6,735 kg
= (6,735*2.2046) lb
= 14,848 lb

Bottom Lid weight = $(\pi/4)*(dia^2)*(length)*density$
= $(\pi/4)*(1.6794^2)*(0.0889)*(7980)$ kg
= 1572 kg
= (1572*2.2046) lb
= 3465 lb

Shell weight = (total wt.) – wt. of (top plug + bottom plate)
= (49,320) – (6735 + 1572) kg
= 41, 013 kg
= (41,013*2.2046) lb
= 90,417 lb

Shell length = (Total length) – length of (Top Plug + Bottom Plate)
= (5.3497) – (0.381 + 0.0889) m
= 4.8798 m

Shell weight (ID Formula) = $(\pi/4)*(OD^2 - ID^2)*(shell\ length)*(density)$
= $(\pi/4)*(1.6794^2 - ID^2)*(4.8798)*(7980)$ kg
= 41,013 kg

Shell internal diameter (ID):

$(1.6794^2 - ID^2) = \{(41,013)/(7980*4.8798)*(\pi)\}*(4)$
= 1.341
ID = $(1.6794^2 – 1.341)^{0.5}$ m
= 1.2163 m
= (1.2163 * 3.281 * 12) in.
= 47.89 in.

Shell wall thickness = (OD – ID)/2
= (1.6794 – 1.2163)/2 m
= 0.2315 m
= (0.2315 * 3.281 * 12) in.
= 9.1165 in.

6.2.2 Calculations for TAD Canister Center of Gravity Location

Center of Gravity locations (along the z-axis) relative to the bottom external surface of the SNF canister.

Bottom Lid Center of Gravity (z-axis) = (3.5 in)/2 = 1.75 in.
= (1.75)/(12*3.281) m = 0.0444 m

Shell Center of Gravity (z-axis) = 3.5 in + (192.13 in)/2 = 99.57 in.
= (99.57)/(12*3.281) m = 2.529 m

Top Lid (Plug) Center of Gravity = 3.5 in + 192.13 in. + (15 in)/2 = 203.13 in.
= (203.13)/(12*3.281) m = 5.159 m

Total Canister Center of Gravity (z-axis) =

= [(1.75 in*3,465 lb)+(99.57 in*90,417 lb)+(203.13 in*14,848 lb)]/108,731 lb
= 110.6 in.
= (110.6)/(12*3.281) m = 2.809 m

Bounding CG location (distance from bottom external surface of the loaded canister) between 103 in. and 123 in. (Reference 2.2.26, Figure C-17)

= (103/12*3.281) m and (123/12*3.281) m

= 2.6161 m and 3.124 m

6.3 REDUCTION OF THICKNESS DUE TO CORROSION

Unless noted otherwise, an upper bound value of the general corrosion rate of 256 nm/year (0.0000101 in./yr)(the 99.99th percentile rate at 150 °C (302 °F)) is used in the calculations (Assumption 3.2.6). Using this corrosion rate for the regulatory period of 10,000 years, the thickness of the outer surface of the waste package outer shell, WP sleeves, and the lids are reduced by 2.56 mm (0.101 in.). Use of corrosion reduction for the OCB components provides a consistent comparison with earlier rock fall calculations. Stress intensities calculated in components that have been thinned by corrosion will be slightly higher than the stress intensities calculated without the corrosion condition applied. Therefore, the application of this corrosion condition provides a worst-case stress intensity value.

The corrosion reduction condition was not applied to Case #8a so that non-conservative stress intensity values in the OCB could be calculated for comparison purposes. Only the lower WP sleeve region was subjected to rock fall for the non-corroded case because the lower WP sleeve region was deemed the worst case orientation during the corroded model simulations. The emplacement pallet plate corrosion has no significant effect on the results of this calculation since the scope of this calculation is limited to reporting the WP structural performance subjected to rock falls, which experiences high stresses only in the vicinity of the region of impact.

Therefore, the initial material thicknesses are used for the emplacement pallet components (Assumption 3.2.6).

6.4 CALCULATION FOR ROCK DIMENSIONS

The rock shape used in this calculation is that of a rectangular prism (see Assumption 3.11 in Ref. 2.2.12). In accordance with the calculations provided in *Drip Shield Structural Response to Rock Fall* (Ref. 2.2.12, Section 5.3), the rock dimensions for this analysis have been derived by scaling the dimensions of the 14.5 MT (31,967 lbs) rock in that Reference as follows:

$d = m_2 / v_2$
$d = m_1 / v_1$

Therefore:
$v_2 / v_1 = m_2 / m_1$

Where:
d = rock density, m = rock mass, and v = rock volume
a, b, c = three different side lengths of a rectangular prism
Subscripts 1 and 2 indicate two rocks of different sizes

The dimensions of a 20.0 MT (44,092 lbs) rock are calculated below:

$v_2 / v_1 = m_2 / m_1 = 20.0 / 14.5 = 1.379$

$v_2 = 1.379 * v_1 = [(1.379)^{1/3} * a_1] [(1.379)^{1/3} * b_1] [(1.379)^{1/3} * c_1]$
$v_2 = [1.113\ a_1] [1.113\ b_1] [1.113\ c_1]$

The dimensions of the 14.5 MT (31,967 lbs) rock are:
$a_1 = 2.5$ m (98.4 in.)
$b_1 = 2.5$ m (98.4 in.)
$c_1 = 1.0$ m (39.4 in.)

Therefore, the dimensions of the 20.0 MT (44,092 lbs) rock are:
$a_2 = 1.113 * a_1 = 1.113 * 2.5 = 2.783$ m (109.6 in.)
$b_2 = 1.113 * b_1 = 1.113 * 2.5 = 2.783$ m (109.6 in.)
$c_2 = 1.113 * c_1 = 1.113 * 1.0 = 1.113$ m (43.82 in.)

Each rock is positioned such that its center of gravity lies directly above the point of impact. The position of the rock is centered over the top of the WP (x = 0) with symmetry about the YZ plane which goes through the WP centerline. Therefore the rock inclination is determined using two dimensions of the rectangular prism:

Rock angle of inclination = $\arctan (c_1 / b_1) = \arctan (1.0 / 2.5) = 21.8°$

Repeating the calculation for a 0.5 MT (1,102 lbs) rock (used in the multiple rock fall simulation) yields the following rock dimensions: a_2 = 0.814 m (32.0 in.), b_2 = 0.814 m (32.0 in.), c_2 = 0.326 m (12.8 in.).

Repeating the calculation for a 2.15 MT (4,740 lbs) rock (used in the multiple rock fall with rockbolt simulation) yields the following rock dimensions: a_2 = 1.323 m (52.09 in.), b_2 = 1.323 m (52.09 in.), c_2 = 0.529 m (20.83 in.).

6.5 FINITE ELEMENT REPRESENTATION

Rock falls may occur both in the preclosure and post-closure periods. For the preclosure period, the drip shields have not yet been emplaced, so rocks may fall onto the emplaced waste packages. Three WP configurations for license application are investigated to determine their structural response to rock fall sequences: the TAD canistered SNF WP (may hold either 21 PWR fuel assemblies or 44 BWR fuel assemblies), a 5-DHLW/DOE SNF Co-disposal Short WP, and a Naval Canistered SNF Long WP (See Assumption 3.1.1). A finite element analysis is performed by using the commercially available LS-DYNA finite element code. Four different axial regions of rock fall impact are evaluated in this study (Figure 3). The first impact region (A) is selected at the WP lower end, directly above the WP-sleeve-to-bottom lid fillet-weld region; the second (C), at mid-length; the third (B), directly above the emplacement pallet support; and the fourth (D), at the WP upper end, directly above the closure-weld region. These regions encompass the range of WP regions that a falling rock could hit the top of the WPs and because all of the rock's kinetic energy is transferred into the WPs, they provide starting regions to determine bounding results for structural evaluations. At some regions, small adjustments are then made to the exact axial impact location to induce maximum wall-averaged stress intensities in the WP OCB.

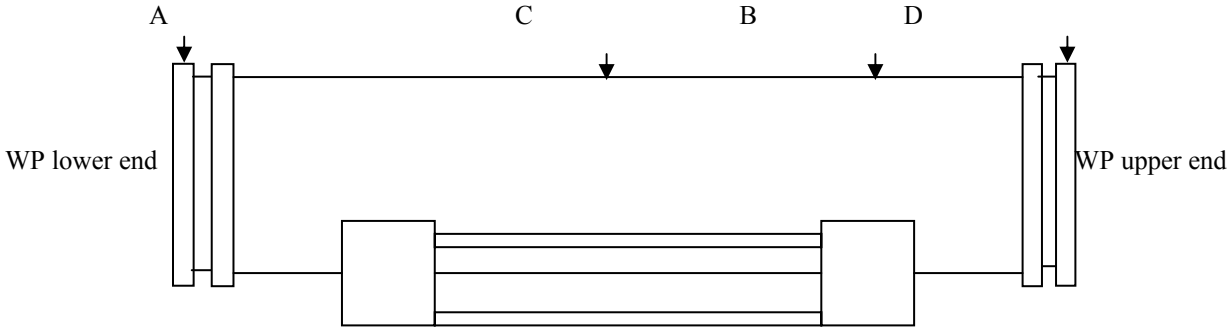

Figure 3. A Simplified Illustration of Rock-WP Impact Regions

One WP configuration is used to determine the most damaging location of impact among the four impact regions. For this purpose, LS-DYNA simulations of the TAD bearing WP are developed for all four impact regions. The results of these calculations suggest that the most

damaging results are obtained when the axial location of the rock impact zone is directly above the trunnion collar sleeve, at the bottom lid fillet-weld region (Case A in Figure 3). Consequently, the rock fall calculations for the remaining waste package configurations are performed for this impact location, which is the most damaging simulation setup used. A list of LS-DYNA simulations performed for this calculation is presented in Table 2.

Table 2. List of LS-DYNA Simulations

Case #	WP configuration	Type of rock fall	Rock Impact Region	Rock mass	Rock Velocity	Rock Kinetic Energy	Notes on FER mesh size	Filename used in LS-DYNA simulations
1	TAD bearing	Single rock fall	Case A	20 MT (22 ton)	10.0 m/s (32.8 ft/s)	1.0 * 10^6 J (737,560 ft·lb$_f$)	Coarse	tada2m1b_coarse.k
2	TAD bearing	Single rock fall	Case A	20 MT (22 ton)	10.0 m/s (32.8 ft/s)	1.0 * 10^6 J (737,560 ft·lb$_f$)	Standard	tada2m1b_std.k
3	TAD bearing	Single rock fall	Case A	20 MT (22 ton)	10.0 m/s (32.8 ft/s)	1.0 * 10^6 J (737,560 ft·lb$_f$)	Very Fine	tada2m1b_refined.k
4	TAD bearing	Single rock fall	Case A	20 MT (22 ton)	10.0 m/s (32.8 ft/s)	1.0 * 10^6 J (737,560 ft·lb$_f$)	Fine	tada2m1b.k
4a	*TAD bearing w/ Inner Vessel at bottom*	*Single rock fall*	*Case A*	*20 MT (22 ton)*	*10.0 m/s (32.8 ft/s)*	*1.0 * 10^6 J (737,560 ft·lb$_f$)*	*Fine*	*tada2m1_IVbot.k*
5	TAD bearing	Single rock fall	Case B	20 MT (22 ton)	10.0 m/s (32.8 ft/s)	1.0 * 10^6 J (737,560 ft·lb$_f$)	Fine	tad_a1m1q1.k
6	TAD bearing	Single rock fall	Case C	20 MT (22 ton)	10.0 m/s (32.8 ft/s)	1.0 * 10^6 J (737,560 ft·lb$_f$)	Fine	tad_a1m8_mid2e.k
6a	*TAD bearing w/ 21PWR mockup*	*Single rock fall*	*Case C*	*20 MT (22 ton)*	*10.0 m/s (32.8 ft/s)*	*1.0 * 10^6 J (737,560 ft·lb$_f$)*	*Fine*	*tad_a1m8_mid2d_21PWRa.k*
7	TAD bearing	Single rock fall	Case D	20 MT (22 ton)	10.0 m/s (32.8 ft/s)	1.0 * 10^6 J (737,560 ft·lb$_f$)	Fine	tada1m1tb.k
8	TAD bearing, no machining of sleeves	Single rock fall	Case A	20 MT (22 ton)	10.0 m/s (32.8 ft/s)	1.0 * 10^6 J (737,560 ft·lb$_f$)	Fine	TADa2m9b.k
8a	*TAD bearing, no machining of sleeves, no OCB corrosion*	*Single rock fall*	*Case A*	*20 MT (22 ton)*	*10.0 m/s (32.8 ft/s)*	*1.0 * 10^6 J (737,560 ft·lb$_f$)*	*Fine*	*TADa2m9b_noCorr.k*
9	TAD bearing	Single rock fall w/rockbolt	Case A	20 MT (22 ton)	10.0 m/s (32.8 ft/s)	1.0 * 10^6 J (737,560 ft·lb$_f$)	Fine	TADa2m1bolt4.k
10	TAD bearing	Single rock fall w/rockbolt	Case B	20 MT (22 ton)	10.0 m/s (32.8 ft/s)	1.0 * 10^6 J (737,560 ft·lb$_f$)	Fine	TAD_a1m1qbolta2.k
11	TAD bearing	Single rock fall w/rockbolt	Case C	20 MT (22 ton)	10.0 m/s (32.8 ft/s)	1.0 * 10^6 J (737,560 ft·lb$_f$)	Fine	TADa1m8bolt_mid2f.k
12	TAD bearing	Single rock fall w/rockbolt	Case D	20 MT (22 ton)	10.0 m/s (32.8 ft/s)	1.0 * 10^6 J (737,560 ft·lb$_f$)	Fine	TAD_a1m1tboltc.k
13	TAD bearing	Multiple rock fall, two rocks	Case A	20 MT (22 ton), 0.5 MT (1102 lb)	9.96 m/s (32.7 ft/s), 6 m/s (19.7 ft/s)	1.0 * 10^6 J (737,560 ft·lb$_f$) Total	Fine	tada2m1b_dbl.k
14	TAD bearing	Multiple rock fall, five w/rockbolt	Case A	5 * 0.43 MT (2.37 ton) Total	4.31 m/s (14.1 ft/s)	2.0 * 10^4 J (14,750 ft·lb$_f$) Total	Fine	TADa2m1bolt4b_multi_2.k
15	Co-Disposal 5DHLW/1DOE SNF	Single rock fall	Case A	20 MT (22 ton)	10.0 m/s (32.8 ft/s)	1.0 * 10^6 J (737,560 ft·lb$_f$)	Fine	5dhlwa2m1.k
16	Co-Disposal 5DHLW / 1DOE SNF, w/ no machining of sleeves	Single rock fall	Case A	20 MT (22 ton)	10.0 m/s (32.8 ft/s)	1.0 * 10^6 J (737,560 ft·lb$_f$)	Fine	5dhlwa2m1_newSleeve.k

For rock mass, velocity, and kinetic energy values, see Assumption 3.2.15
Case numbers in italics are the supplement simulations that were run as sensitivity cases.

In the initial simulations, the orientation of the machined WP sleeves for trunnion collar attachments are adjusted at both ends of the WP in such a way that the minimum thickness of the sleeve is used in the region of the rock impact. The reason for this is to provide less material to absorb impact energy and, therefore, obtain conservative stress results. Later simulations were made for smooth WP sleeves that would not attach to trunnion collars (Case #8 and Case #8a). The impacting rock block is prone to large deformations due to its low compressive strength compared to Alloy 22. For any impact scenario that causes the rock to impact onto the sharp edge of the WP sleeve, the rock is anticipated to locally deform and transfer part of its energy onto the thick section of the sleeve. Such behavior of local deformation is observed in both simulations where a WP sleeve is hit (Case A (lower sleeve) and Case D (upper sleeve)). The rock deforms such that it matches the contacted shapes of the waste package sleeve's sidewalls (see Figures 10 and 11). Therefore, the use of the thin section of the waste package sleeve as the rock impact location provides a conservative approach to these finite element evaluations. Because of model instabilities that arose when the impacting rock attempted to plastically form to the 90 degree angles of a machined WP sleeve, the modeled sleeve was modified for stabilization purposes only. In the region of rock impact, the thick portion of the WP sleeve was modified to rise up from the thin portion of the sleeve at a 45 degree angle instead of the designed 90 degree angle. This modification was done in a way that removed material from the thick portion of the WP sleeve so the modification is conservative. Later simulations were based on WP sleeves without machining for trunnion collars.

The rock fall evaluations do not result in significant interaction of the inner shell structure with the inner shell contents, such as the canisters or the basket structure. Therefore, the effects of different basket types and orientations are not studied in this calculation.

For single rock fall evaluations, a total of 17 three-dimensional half-symmetry FERs of the WP emplaced on the EP, and the rock (also half-symmetry), are developed in LS-DYNA. All 17 single rock fall evaluations use the credible bounding rock mass and kinetic energy scenario to size the impacting rock (20 MT (44,092 lb) rock with maximum $1.0 * 10^6$ J (737,560 ft·lb$_f$) kinetic energy, see Assumption 3.2.15 and Table 1) (see Figure 4 for a typical FER). Of these 17 single rock fall evaluations, 15 simulations used a TAD canister bearing WP configuration (Ref. 2.2.30 thru Ref. 2.2.32) and two simulations used a 5DHLW/1DOE SNF co-disposal short WP configuration (Ref. 2.2.47 thru Ref. 2.2.49). The corrosion condition described in Section 6.3 is applied in all cases except Case #8a.

FERs are developed by using the dimensions provided in Section 6.2, Section 6.3, and References 2.2.30 thru 2.2.52. To reduce the computer execution time while preserving all features of the problem relevant to the structural calculation, the rock is set in a position just before impact and given an appropriate initial impact velocity. The input values for rock impact velocity and rock block size for single and multiple rock fall simulations are specified in Assumption 3.2.15, which also provides the basis for these inputs. Using the relation: kinetic energy = mass * $(\text{velocity})^2 / 2$, a 20.0 MT (44,092 lbs) rock with maximum $1.0 * 10^6$ J (737,560 ft·lb$_f$) kinetic energy results in a velocity of 10.0 m/s (32.8 ft/s) (see Assumption 3.2.15 and Table 1).

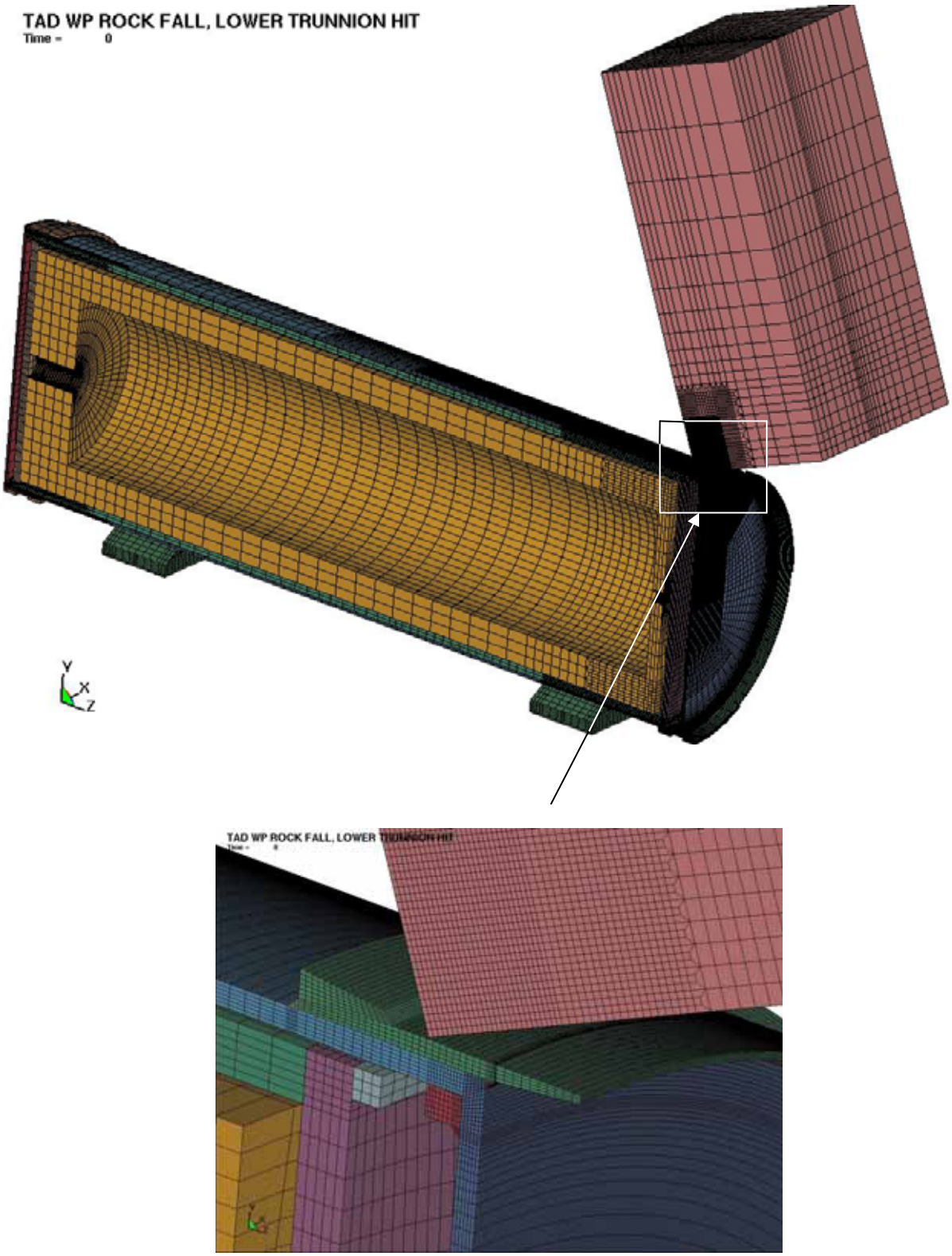

Figure 4. Single Rock Fall Finite Element Mesh for TAD Bearing WP

Depending on the rock fall region, the inner vessel is repositioned axially within the OCB to maximize the stresses the rock strike will produce in the OCB. When the rock fall region is on the lower WP sleeve then the inner vessel and TAD canister are positioned at the upper end of the WP cavity, only a loose fit gap distance (11.1 mm) away from the upper lid of the OCB at the top of the waste package. When the rock fall region is on the upper WP sleeve then the inner vessel and TAD canister are positioned to the opposite end of the WP cavity, in contact with the interface ring and support ring at the bottom of the waste package. The mid package rock fall region scenario, Case #6, and the quarter point rock fall region scenario, Case #7, have no sensitivity to the position of the inner vessel, in these cases the inner vessel and TAD canister are simply placed in the middle of the OCB cavity. During a simulation the inner vessel is free to move within the OCB interior, as well as the TAD canister within the inner vessel cavity. Case #6a is a rerun of Case #6 with the exception that an approximation of a 21-PWR basket and assemblies are modeled inside the TAD canister. The exact geometries of the PWR Fuel assemblies are simplified in the FER (Assumption 3.2.16). These fuel assemblies are assumed to be made of 304 SS (Assumption 3.2.17) and conservative mass and enveloping dimensions are used in the calculations (Assumption 3.2.16).

These FERs are used in LS-DYNA to perform a transient dynamic analysis of rock fall. The rock shape used in this analysis is consistent with the rock geometry and dimensions obtained and used in previous rock fall structural analyses (Assumption 3.2.14). The angle of rock inclination with respect to the WP is adjusted such that the center of gravity of the rock is directly above the initial contact region (see Assumption 3.2.14). This configuration is conservative, since the kinetic energy of the rock is transferred to WP strain energy over a relatively small impact volume. The FER of the falling rock is divided into three regions: a small finely-meshed impact region, and intermediate region of less mesh refinement, and a large coarsely-meshed region for the remaining portion of the rock. These three regions of the rock have a tied-node interface with each other to ensure that the rock will behave as one continuous part during the simulations. The finely-meshed portion of the rock is necessary to capture the deformation of the rock in the localized region of impact and simulate the crushing of the rock expected in that region.

LS-DYNA “standard” contact algorithms are used to represent contacts between: rock and WP, OCB and inner vessel, OCB and emplacement pallet, inner vessel and TAD canister, and any contact interactions between the TAD canister contents if they are modeled. In the absence of more appropriate data, the dynamic friction coefficients for all WP component contacts are assumed to be 0.4 (see Assumptions 3.2.10 and 3.2.11). It is assumed that the functional friction coefficient and the static friction coefficient are equal to the dynamic friction coefficient (see Assumption 3.2.13). For the rock on WP contact, the dynamic friction coefficients are assumed to be 0.525 (Assumption 3.2.12). For the rock on WP contact, again, the functional friction coefficient and the static friction coefficient are assumed equal to the dynamic friction coefficient (see Assumption 3.2.13). To increase solution stability, the contact stiffnesses are doubled and the contact viscous damping is set to 30%. A very small amount of structural damping (*DAMPING_PART_STIFFNESS, Coef = 0.0001) was used to stabilize any high frequency response without any expected affect on the major (low frequency) responses sought after in the OCB.

The mesh of the FER (see Figure 4 for example) is appropriately generated and refined in the contact region according to standard engineering practice and the methodology described in Section 6.2.3 of Reference 2.2.24.

A list of all LS-DYNA simulations, their corresponding waste package configurations, rock fall types, WP regions of impact, rock masses, velocities, and kinetic energy values are presented in Table 2. The multiple rock fall scenarios involve the striking of a single region of the WP by either a two rock scenario, Case #13, or by a scenario involving a rockbolt with five rocks attached to it, Case #14. The multiple rock scenarios, Cases #13 and #14, have a description in Section 6.5.2. Table 2 also lists the single rock with a rockbolt scenarios, Cases #9 through #12, which conceptualize a rockbolt inside the falling rock and that the rockbolt is positioned to transfer the most energy from the falling rock onto the OCB as possible. The rockbolt is the only difference between the cases with rockbolt and the cases without rockbolt. Section 6.5.1 discusses the details of the rockbolt FER cases.

Table 2 also provides a quick-reference summary of the different case simulations that were run and relates those case numbers to the electronic file names in Attachment I.

6.5.1 Rock with Rockbolt

An addendum to the single rock fall scenario is a rock fall with imbedded rockbolt scenario. In the emplacement drifts, the groutless Super Swellex rockbolt (Assumption 3.1.3 and Reference 2.2.5, Section 7) is the recommended rockbolt for emplacement drift ground support; see Figure 5 (Ref 2.2.29, pg. 14). The Super Swellex rockbolt is hollow with 3mm thick tube walls fabricated from a Type 316 stainless steel or equivalent in order to ensure longevity (Reference 2.2.5, Section 7). The length of the recommended Super Swellex rockbolt is 3 m (118 in.)(Reference 2.2.5, Section 7). For the FER, the face plate is modeled as flat without the dome near the rockbolt hole. The rockbolt bushing head that protrudes out past the rockbolt face plate has 6mm (0.24 in.) thick tube walls to account for the constriction of the rockbolt tube walls inside of the bushing. Also, while the contact surfaces between the rock and rockbolt include friction (Assumption 3.2.12), the contact between the rockbolt and rock surface is not preloaded. So that the initial contact of the rockbolt head on the OCB would conservatively include the full mass of the rock behind the rockbolt, the rock nodes at the tail end of the rockbolt were fused to the rockbolt. The typical FER for the rockbolt in the falling rock scenario is shown in Figures 6 and 7.

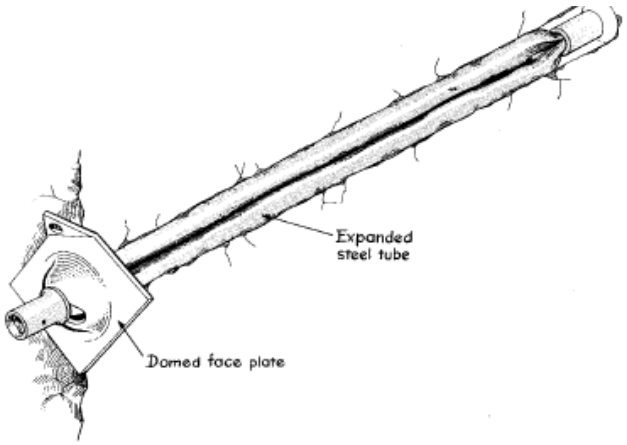

Source: Stillborg 1994, p. 14.

Figure 5. A Typical Swellex Rockbolt

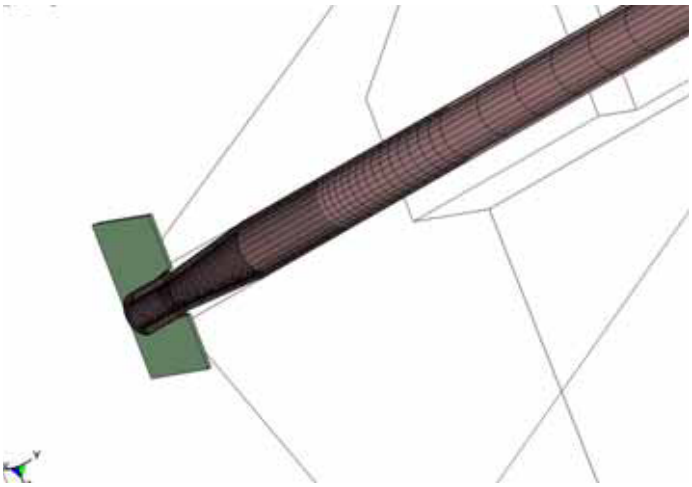

Figure 6. FER Conceptualization of Swellex Rockbolt in Falling Rock, Half Symmetry

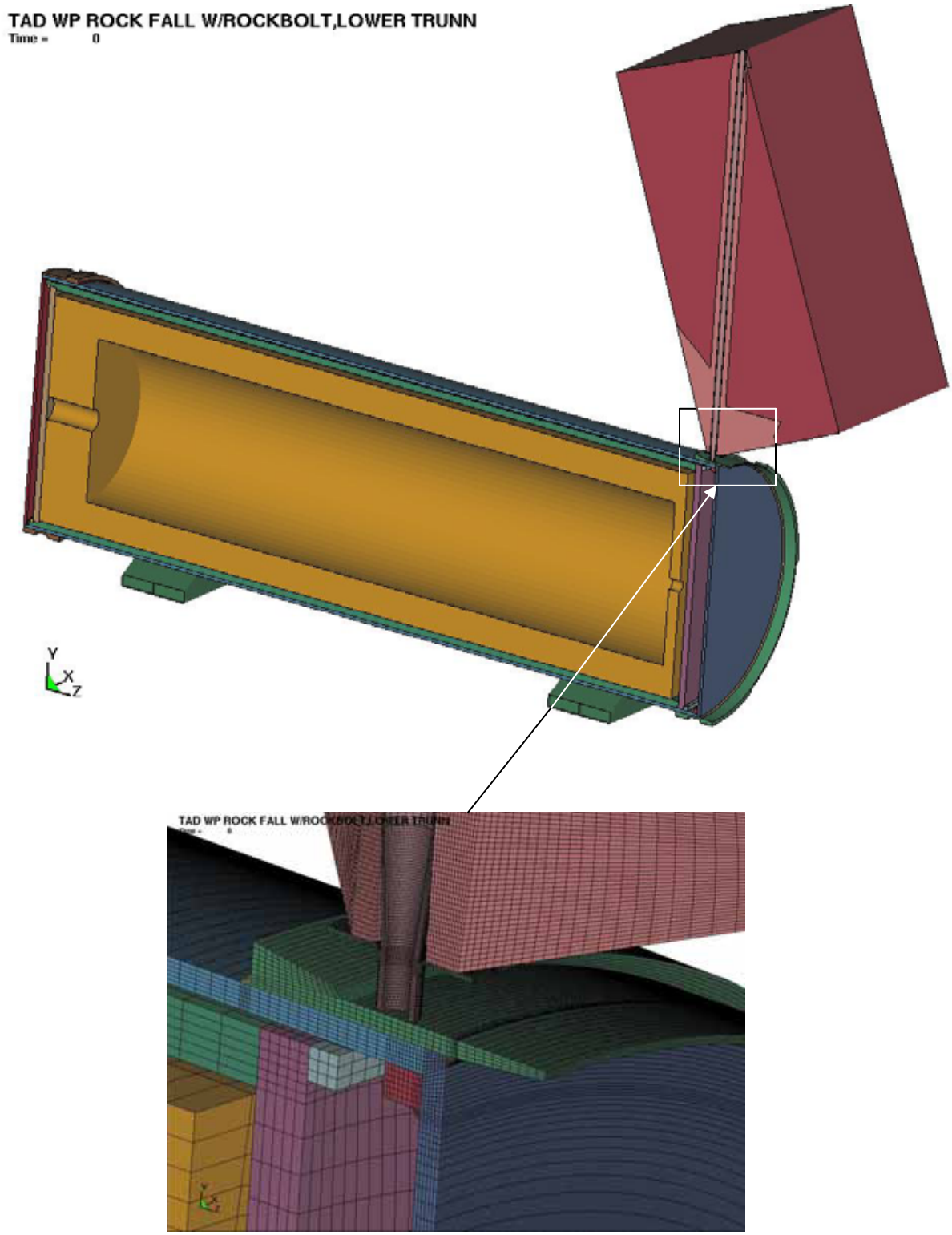

Figure 7. Rock Fall FER, 20 MT (22 ton) Rock with a Rockbolt

6.5.2 Multiple Rock Fall Evaluations

Two additional simulations are performed to determine the response of the WP components to multiple rock falls onto the same region of the WP. Specifically, the effect of multiple rock falls on the wall-averaged stress intensity and effective plastic strain history of the OCB when the rocks impact the same region of the WP.

6.5.2.1 Dual Rock Fall Scenario

The first of the multiple rock fall scenarios is the dual rock fall case (Table 2, Case 13) where the same location is struck by two separate rocks. For the dual rock fall case, the TAD bearing WP with the "Rock Only" impact scenario that produced the highest OCB stress intensities is selected (Table 4, Case 4) as the rock fall region to use for the dual rock fall case. Therefore, the results of this dual rock fall case are bounding for all waste package rock fall region scenarios.

The FER of the WP of the dual rock fall scenario is generally the same as the one used in the single rock fall simulations, but it is modified to have the WP impacted by two distinctly different rocks. The dual rock fall case is modeled as a rock of the credible bounding mass size, 20MT (44,092 lbs), followed by a rock of average expected rock mass as described in Ref. 2.2.28, Section 6.4.5.2.4. Since the total kinetic energy of both rocks must sum to credible bounding kinetic energy level of $1.0*10^6$ Joules (737,560 ft·lb$_f$) the approach taken was to reduce the velocity of the 20MT (44,092 lbs) rock such that the sum of the kinetic energy of an average rock plus the now slower 20MT (44,092 lbs) rock summed to $1.0*10^6$ Joules (737,560 ft·lb$_f$) (Assumption 3.2.15 and Section 6.4.5.2.5 of Ref. 2.2.28). For the purposes of this analysis the second rock is modeled to have a mass and velocity that is close to, but slightly larger and faster than the average expected rock fall mass and velocity in the nonlithophysal zone (Ref 2.2.28, Table 2, Table 6, and Section 6.4.5.2.4). The average rock fall masses range between 220 and 430 kg (485 and 948 lbs) (Ref. 2.2.28, Table 6), and the mean rock fall kinetic energy range of 1,300 to 3,000 J (959 to 2,210 ft·lb$_f$) (Ref. 2.2.28, Appendix A), which together equates to the expected mean rock fall velocities ranging from 3.4 to 3.7 m/s (11.2 to 12.1 ft/s). The small, second rock modeled in the dual rock fall analysis is larger than the average expected rocks at 500 kg (1,102 lbs) (Ref. 2.2.28, Figure 10 and Section 6.4.5.2.4) and is modeled with a faster than expected velocity with an impact velocity of 6 m/s (19.7 ft/s), for a kinetic energy value of 9,000 J (6,640 ft·lb$_f$). Using the remaining kinetic energy (1,000,000 J minus 9,000 J (737,560 ft·lb$_f$ minus 6,640 ft·lb$_f$)) for the 20 MT (44,092 lb) rock that is used in the dual rock fall scenario, slows the large rock impact velocity to 9.955 m/s (32.66 ft/s).

The starting positions of these two rocks with distinctly different masses and velocities are set such that both rocks will fall on the same region of the WP but the second rock fall occurs at a slightly later time. The delayed time the second rock takes to fall on the WP allows the effects of the first rock fall to approach a steady-state and for the rock to move off of the WP. To accomplish the second rock fall impact on the same WP region just after the first rock fall has bounced off of the WP it is necessary for the two rocks to occupy the same physical space in the model, but there are no connections or contacts between the two rocks The FER of this simulation is depicted in Figure 8.

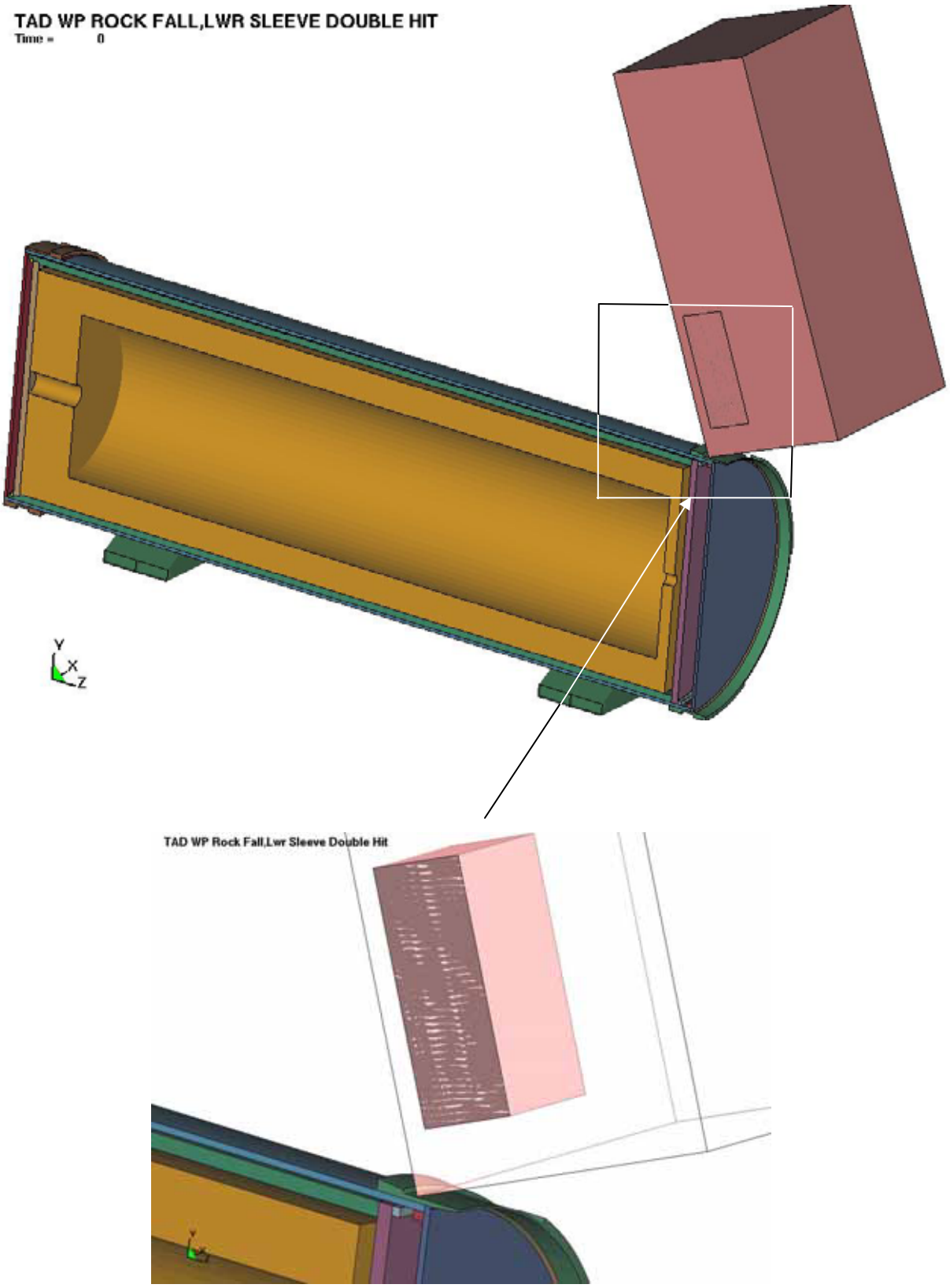

Figure 8. Multiple Rock Fall Scenario FER, 20MT (44,092 lb) Rock Followed by a 0.5 MT (1,102 lb) Rock

6.5.2.2 Multiple Rocks Tied By Rockbolt Scenario

Another postulated configuration for the multiple rock fall scenario is with several rocks connected to each other by a single ground support rock bolt (Ref. 2.2.28, Section 6.4.5.2.4). Considering that the upper range of the average expected nonlithophysal rock mass is 430 kg (948 lbs) (Ref. 2.2.28, Table 6), a standard 3 m (118 in.) Swellex Rock Bolt (Ref. 2.2.5, Section 7) can connect as many as five nonlithophysal rocks of average expected size. The five rock per rock bolt estimate calculated using a simple spherical rock shape approximation, the average expected rock mass, and a rock density of 2411 kg/m^3 (0.0871 lb/in^3) (Assumption 3.2.20) to get spherical rocks of diameter 0.698 m (27.5 in.) in which five could linearly attach to a 3 m (118 in.) rock bolt. A simplified conceptualization of this multiple rock fall scenario is to model the five rocks connected by the rockbolt as a single prismatic rock of 2.15 MT (4,740 lbs) in which the prism side lengths are calculated in Section 6.4, the FER for this conceptualization is shown in Figure 9. Considering that the upper end of range of average expected nonlithophysal rock fall has a kinetic energy of 3,000 J (2,210 $ft \cdot lb_f$), these rockbolt tied rocks would have a total kinetic energy of 5 x 3,000 J = 15,000 J (11,060 $ft \cdot lb_f$). To the upper end of the average expected total kinetic energy of 15,000 J (11,060 $ft \cdot lb_f$) another 5,000 J (3,690 $ft \cdot lb_f$) of kinetic energy was added, resulting in a 33% increase for a total kinetic energy of 20,000 J (14,750 $ft \cdot lb_f$). The additional kinetic energy will result in a faster impact velocity and is a conservative assumption for the multiple rocks on a rockbolt scenario (Assumption 3.2.15, Table 1). In the multiple rock fall scenario, where the rocks are tied by a rockbolt, the impact velocity used during the simulation is 4.31 m/s (14.1 ft/s) (0.5 x 2150 kg x V^2 = 20,000 J) (Assumption 3.2.15, Table 1).

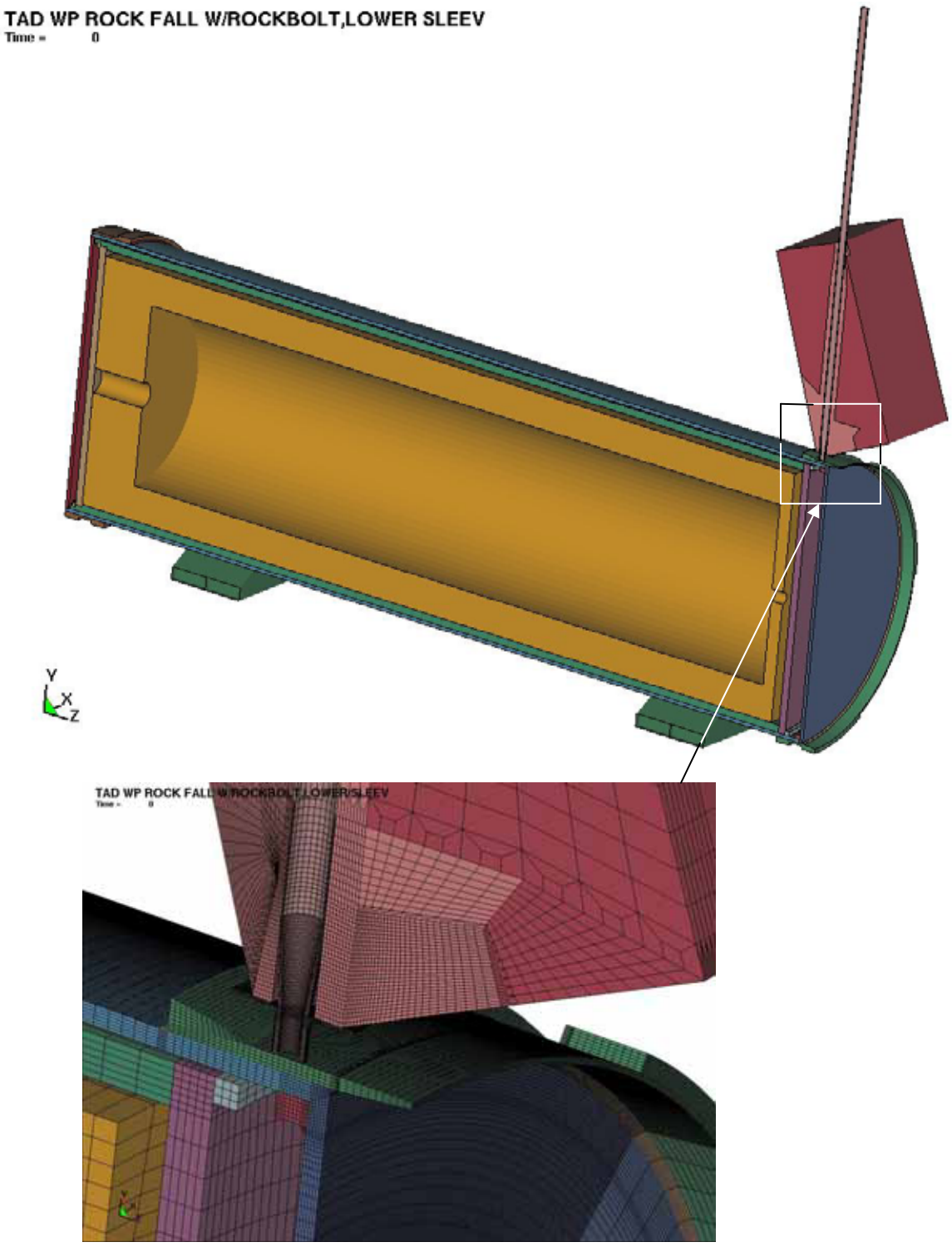

Figure 9. Multiple Rock Fall FER, Five 0.43MT (948 lbs) Rocks on a Rockbolt

7. RESULTS AND CONCLUSIONS

The simulation stress results from LS-DYNA solutions are available in terms of maximum shear stress, but not ASME Code stress intensities. Since the stress intensities are desired, the results need to be translated appropriately. The maximum shear stress is one-half the difference between maximum and minimum principal stresses. Stress intensity is the difference between maximum and minimum principal stress. Therefore, the reported values of maximum shear stress are multiplied by two in order to obtain stress intensity values.

7.1 MESH AND TIME STEP VERIFICATION

An initial study of the FER mesh for the 20 MT (44,092 lb), 10 m/s (32.8 ft/s) rock fall on the TAD Bearing WP at location A (See Figure 3) is performed to verify the objectivity of the mesh, i.e., that the calculation results are not mesh-sensitive. Table 3 shows the element wall-averaged (EWA) stress intensity (SI) of comparable wall sections for four different FER meshes. The EWA SIs presented in Table 3 are each from the same location on the OCB bottom lid (identified by surface element number) in the region of maximum structural response.

The first (coarse) mesh in Table 3 is developed by following the guidance in *Waste Package Component Design Methodology* (Ref. 2.2.24, Section 6.2.3). The standard mesh is a refined version of the coarse mesh, where in the region of interest (OCB lower lid) the mesh is refined in the angular coordinate direction. The bottom lid of the OCB is the critical structural component for reporting maximum structural response for the governing loading. The volumes and stress values for each element are obtained from the post-processing of LS-DYNA simulations. The change in the waste package element volume between the coarse and standard mesh is 67%. The change in EWA SI for the elements in the same location is 9%, which indicates that the change in EWA SI is not within the tolerance described in the Reference 2.2.24, Section 6.2.3. The mesh is again refined to obtain a “fine” mesh, this time the refinement is performed in the radial (outward from the center of the circular lid) direction. In the region of interest, the change in volume and EWA stress magnitudes between the standard and fine mesh simulations are 30% and 4%, respectively. The “fine” mesh is further refined, this time in the axial (lid thickness) direction to make a “very fine” mesh. In the region of interest, the change in volume and EWA stress magnitudes between the fine and very fine mesh simulations are 25% and <1%, respectively. In accordance with the methodology described in Reference 2.2.24, Section 6.2.3, the “fine” mesh is deemed the optimal mesh and a similar mesh density is used for all simulations.

Table 3. Mesh Sensitivity Study Comparisons

Coarse Mesh (Case #1)		Standard Mesh (Case #2)		Change from Coarse Mesh
Element # 52974 (OCB bottom lid, at symmetry plane)	Volume 1.83E-07 m^3 (0.0112 in^3)	Element # 96228 (OCB bottom lid, at symmetry plane)	Volume 6.11E-08 m^3 (0.00373 in^3)	67%
	EWA SI 497 MPa (72.1 ksi)		EWA SI 542 MPa (78.6 ksi)	9%
Standard Mesh (Case #2)		Fine Mesh (Case #4)		Change from Standard Mesh
Element # 96228 (OCB bottom lid, at symmetry plane)	Volume 6.11E-08 m^3 (0.00373 in^3)	Element # 131583 (OCB bottom lid, at symmetry plane)	Volume 4.29E-08 m^3 (0.000262 in^3)	30%
	SI 542 MPa (78.6 ksi)		SI 562 MPa (81.5 ksi)	4%
Fine Mesh (Case #4)		Very Fine Mesh (Case #3)		Change from Fine Mesh
Element # 131583 (OCB bottom lid, at symmetry plane)	Volume 4.29E-08 m^3 (0.000262 in^3)	Element # 138873 (OCB bottom lid, at symmetry plane)	Volume 3.22E-08 m^3 (0.000196 in^3)	25%
	SI 562 MPa (81.5 ksi)		SI 558 MPa (80.9 ksi)	<1%

SI: Stress intensity

7.2 EVALUATION

The results presented in Table 4 refer to the nineteen simulations specified in Table 2. The corresponding case numbers help identify each case between Tables 2 and 4. Table 4 contains the maximum calculated element wall-averaged (EWA) stress intensity (SI) values in the outer corrosion barrier (OCB) of the waste packages, as well as a comparison of the EWA SI against the true tensile strength of the OCB material. A comparison between the maximum calculated EWA SI and 0.7 times the true tensile strength of Alloy 22 (0.7 σ_u) is provided in Table 4 to determine if the first condition of acceptance is met of the failure criterion described in Ref. 2.2.24, section 6.2.4. The results indicate that the ratio (SI / 0.7 σ_u) is less than 1.0, i.e., the maximum EWA SI at any point in the outer shell and lids does not exceed 0.7 times the true tensile strength of Alloy 22.

Table 4. Maximum EWA Stress Intensity in the WP Outer Corrosion Barrier

Case #	Case Summary	Max EWA SI, Start Element	EWA SI (MPa (ksi))	0.7 σ_u	EWA SI / 0.7 σ_u
1	TAD, Lower Sleeve Rock Fall, Rock Only – Coarse	E52974	497 (72.1)	0.7 * 971 MPa = 680 MPa (0.7 * 141 ksi = 98.6 ksi) (Section 6.1.2, Alloy 22 @ RT)	0.73
2	TAD, Lower Sleeve Rock Fall, Rock Only – Standard	E96228	542 (78.6)		0.80
3	TAD, Lower Sleeve Rock Fall, Rock Only – Very Fine	E138378	559 (81.1)		0.82
4	TAD, Lower Sleeve Rock Fall, Rock Only	E139980	573 (83.1)		0.84
4a	*TAD, Lower Sleeve Rock Fall, Inner Vessel at Bottom, Rock Only*	*E140112*	*456 (66.1)*		*0.67*
5	TAD, Quarter Point Rock Fall, Rock Only	E182421	583 (84.6)		0.86
6	TAD, Mid Point Rock Fall, Rock Only	E174051	584 (84.7)		0.86
6a	*TAD, WP Mid Point Rock Fall, w/21PWR internals, Rock Only*	*E174129*	*514 (74.5)*		*0.76*
7	TAD, Upper Sleeve Rock Fall, Rock Only	E49026	400 (58.0)		0.59
8	TAD, Lower Sleeve Rock Fall, no machining of sleeve, Rock Only	E140100	556 (80.6)		0.82
8a	*TAD, Lower Sleeve Rock Fall, no machining of sleeve, no corrosion, Rock Only*	*E140100*	*452 (65.6)*		*0.66*
9	TAD, Lower Sleeve Rock Fall, Rock w/Swellex Bolt	E140114	622 (90.2)		0.91
10	TAD, WP Quarter Point Rock Fall, Rock w/Swellex Bolt	E183240	606 (87.9)		0.89
11	TAD, WP Mid Point Rock Fall, Rock w/Swellex Bolt	E174048	604 (87.6)		0.89
12	TAD, Upper Sleeve Rock Fall, Rock w/Swellex Bolt	E57492	462 (67.0)		0.68
13	TAD, Lower Sleeve Rock Fall, Multiple Rock Falls	E139980	568 (82.4)		0.84
14	TAD, Lower Sleeve Rock Fall, Multiple Rock Falls w/Swellex bolt	E140112	416 (60.3)		0.61
15	Co-Disposal, Lower Sleeve Rock Fall, Rock Only	E131088	622 (90.2)		0.91
16	Co-Disposal, Lower Sleeve Rock Fall, no machining of sleeve, Rock Only	E140112	564 (81.8)		0.83

Case numbers in italics are the supplement simulations that were run as sensitivity cases.

The rock fall scenarios that involve contact with a WP sleeve were modeled using an earlier design of the WP sleeve that included machining for the possible attachment of a trunnion collar (e.g., see Ref. 2.2.57, Section 4.2 and Ref. 2.2.58 thru Ref. 2.2.60). In Case #8 and Case #16 a structural response evaluation of rock fall on a WP sleeve of later design that did not include the machining for the trunnion collar attachment was performed (Ref. 2.2.30 thru Ref. 2.2.32, as well as Ref. 2.2.47 thru Ref. 2.2.49). For the TAD bearing WP, the OCB EWA SI calculated in the lower lid due to a rock fall on the lower WP sleeve was reduced by 6% for the later WP

sleeve design that did not have the trunnion collar attachment machining. Figure 14 shows the comparison of OCB lower lid EWA SIs for the WP sleeve with the trunnion attachment cutouts (Case #4) and for the WP sleeve without the cutouts (Case #8), for the TAD bearing WP during the lower WP sleeve rock fall scenario. Figure 15 shows the comparison of OCB lower lid EWA SIs for the WP sleeve with the trunnion attachment cutouts (Case #15) and for the WP sleeve without the cutouts (Case #16), for the 5DHLW/DOE Co-disposal WP.

As described in Section 6.3, the thicknesses of the OCB components are reduced by an amount equivalent to 10,000 years of corrosion at the upper bound of the general corrosion rate for Alloy 22. Case #8a is a repeat of Case #8 with the difference that the thickness of the OCB is not reduced by the corrosion condition described in Section 6.3. Figure 16 shows the structural response to rock fall on the lower sleeve of the TAD bearing WP, both with and without the corrosion condition applied. In both cases the rock fall is on the lower WP sleeve without trunnion collar machining.

The calculated OCB EWA stress intensities for the multiple rock fall simulation identified as Case #13 in Table 4 and presented in Figure 17 show that the ASME stress failure criterion is satisfied, i.e. (SI / 0.7 σ_u) is less than 1.0. In addition to the SI based analysis, the multiple rock fall is evaluated in terms of the maximum EWA effective plastic strain in case of a cumulative effect of strain on the bottom lid. Figure 18 shows that the initial rock impact produces a maximum effective plastic strain in the bottom lid of 0.143, and that the second rock (which makes contact at 40ms) does not create enough distortion in the OCB to plastically strain the bottom lid. The onset of effective plastic strain shown in Figure 18 has a peak rate of 20 s^{-1}, which is consistent with Assumption 3.2.3 in indicating that only a minor strengthening of the material will occur due to the rate of strain experienced during the initial rock fall. The multiple rock fall simulation identified in Case #14 of Table 4 addresses the five falling rocks conservatively modeled with a rock bolt connection to all five rocks as a single impact instead of five individual impacts. Therefore, a cumulative affect on plastic strain in the regions of interest is not expected for this case.

The calculated OCB stress intensities in the cases where the rock strikes the lower WP sleeve were consistently higher than the cases where the rock strikes the upper WP sleeve. Two factors that contribute to this are the difference in sleeve placement between the top and bottom of the WP, where the upper sleeve is completely over the OCB but the lower sleeve overhangs the OCB by 0.102 m (4 in.), one third its length (Ref. 2.2.30 thru Ref. 2.2.32). This 0.102 m (4 in.) overhang of the WP sleeve at the lower end of the WP causes an inward bending direction of the WP sleeve versus an outward bending observed at the upper WP sleeve rock falls, Figures 10 and 11 show this bending difference. Also, in both the upper and lower WP sleeve rock fall cases the inner vessel was positioned in the OCB cavity away from the rock strike point to reduce the structural assistance the inner vessel provides the OCB. Differences in OCB stress intensity between the upper and lower WP sleeve rock fall cases can be attributed to the WP support ring and interface ring (Ref. 2.2.30 thru Ref. 2.2.32) limiting the distance the inner vessel can be repositioned during the upper WP sleeve rock fall case, but not limiting the inner vessel repositioning and adding little support to the OCB during the lower WP sleeve rock fall case. Case #4a is a rerun of Case #4 with the exception that the inner vessel is positioned flush up against the interface ring, which is also flush against the support ring. As can be seen from

Table 4, this significantly improves the structural response of the OCB during the lower WP sleeve rock fall.

In the rock fall on the middle of the WP, Case #6, the TAD canister is calculated to be deformed inward as much as 0.1234 m (4.86 in.). Figure 12 shows the middle WP rock fall, Case #6, 22 ms after the initial impact of the falling rock on the WP. Such deformation would encounter structural support from the contents of the TAD canister, but designs for the contents of the TAD canister have not yet been established. In Case #6a the rock fall on the middle of the WP scenario was reran with a conceptualization of a 21 PWR basket and assembly in the TAD canister. The conceptualization of the TAD canister 21 PWR internals is based on a previous WP basket design (Ref. 2.2.50 thru Ref. 2.2.52). The inclusion of TAD canister internal structures (fuel assemblies and basket) provides structural support during the rock fall and significantly reduces the stress intensities calculated for the OCB (Table 4). Figure 13 shows the middle WP rock fall scenario with a FER of a 21-PWR basket with SNF inside the TAD canister, Case #6a, 22 ms after the initial impact of the falling rock on the WP. Figure 19 shows EWA stress intensities at the same element location for both the mid WP rock fall scenario without canister internal structures, Case #6, and the mid WP rock fall scenario with canister internal structures, Case #6a. As can be seen in Figure 19, the 21-PWR basket modeled in Case #6a does provide structural support during a mid package rock fall that reduces the peak EWA SI.

Because the highest structural response to rock fall was observed when a rock struck the lower WP sleeve of the TAD Bearing WP, both rock fall cases for the 5 DHLW/DOE SNF Co-disposal WPs involved a rock fall strike on the lower WP sleeve. Case #15 modeled the original WP lower sleeve which was machined to allow for a trunnion collar attachment (Ref. 2.2.58 thru Ref. 2.2.60). Case #16 modeled a WP sleeve which did not include any machining for a trunnion collar attachment (Ref. 2.2.47 thru Ref. 2.2.49). The structural response in both of the co-disposal WP rock fall simulations was slightly higher than in the TAD bearing WP simulation, but still well below the failure criterion screen of $0.7\sigma_u$. The small difference in OCB SI calculated for the Co-disposal WP and the TAD bearing WP may be due to the Co-disposal WP OCB design having a larger radius than the TAD bearing WP OCB.

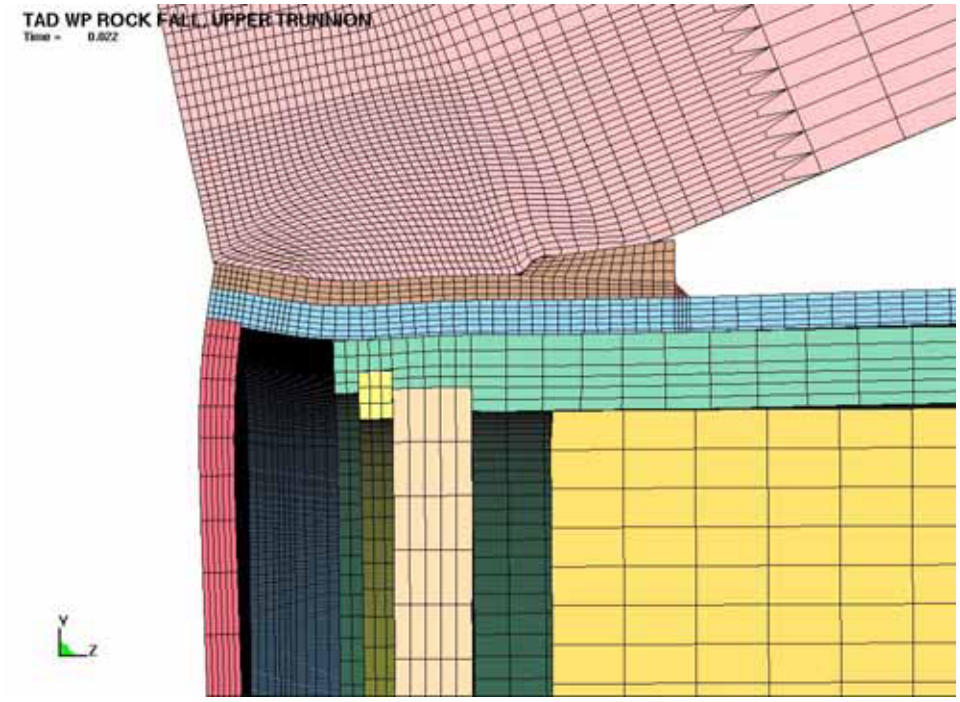

Figure 10. Upper WP Sleeve Rock Fall FER, 20 MT (22 ton) Rock, 22 ms After Impact

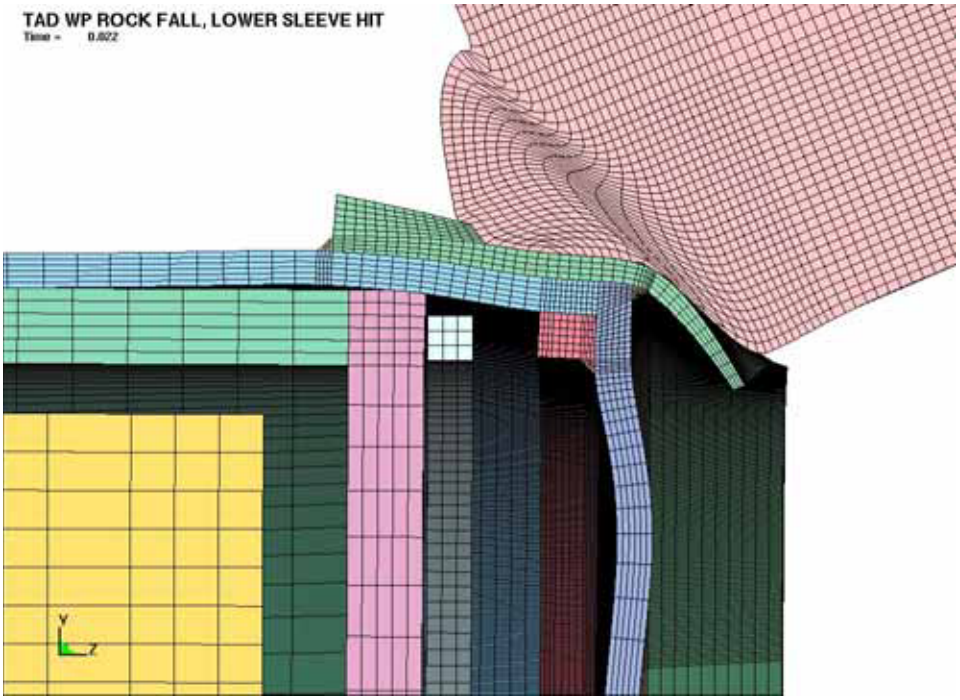

Figure 11. Lower WP Sleeve Rock Fall FER, 20 MT (22 ton) Rock, 22 ms After Impact

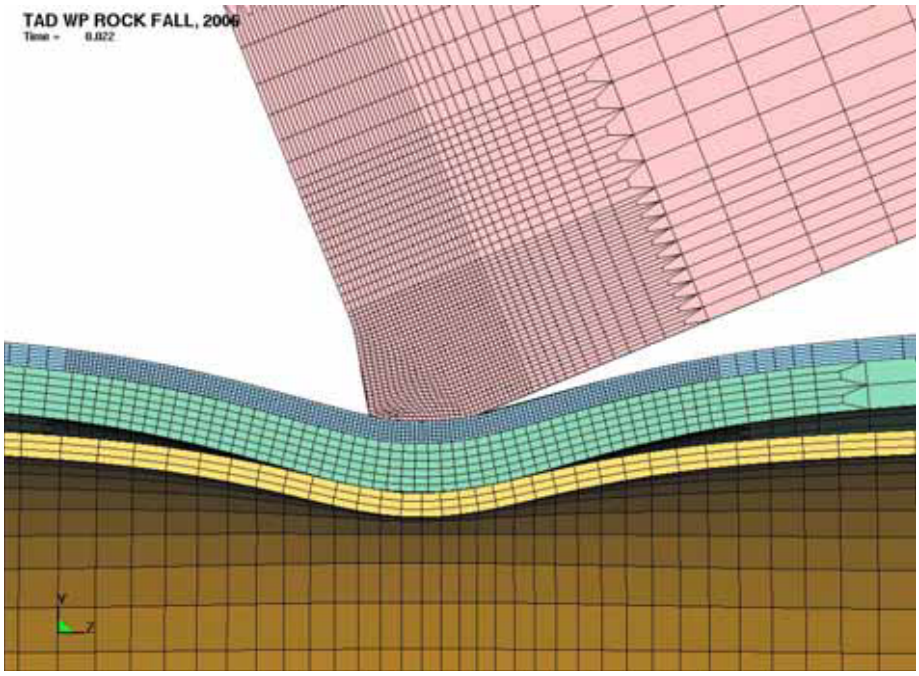

Figure 12. Mid WP Rock Fall FER, 20 MT (22 ton) Rock, 22 ms After Impact

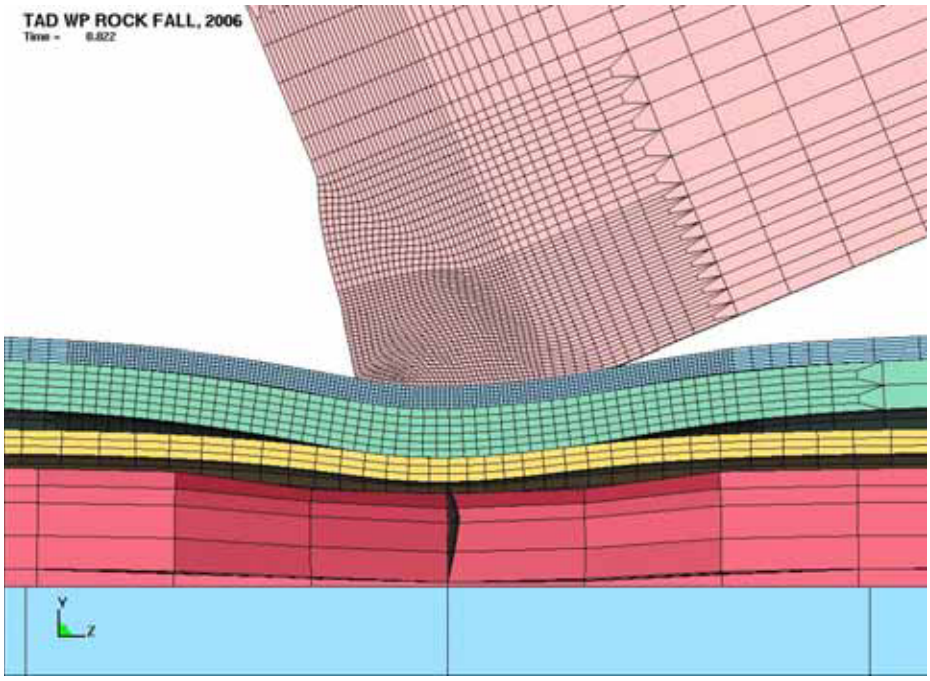

Figure 13. Mid WP Rock Fall FER with conceptual 21-PWR internals, 20 MT (22 ton) Rock, 22 ms After Impact

7.3 SUMMARY AND CONCLUSION

The output values are reasonable for the given inputs in this calculation. Where uncertainties are not specified, they are taken into account by consistently using the most conservative approach; the calculations, therefore, yield a bounding set of results. The results are suitable for assessment of the stresses in the waste packages. The results presented in Table 4 indicate that the maximum EWA SI at any point in the outer shell and lids does not exceed 0.7 times the true tensile strength of Alloy 22. The structural response of the TAD bearing WP and the Co-disposal WP due to rock fall have satisfied the first condition of acceptance of the failure criterion described in Ref. 2.2.24, section 6.2.4 so no further analyses are required. Therefore, the resulting effects of the maximum element wall-averaged stress intensity in the waste package OCB due to credible bounding rock falls is within acceptable levels and does not cause failure.

ATTACHMENT I.
DIRECTORY LISTING (DATA DVD) OF ELECTRONIC FILES

Table 5. Attachment I: File Directories, Names, Dates, Times, and Sizes

Directory	Name	Date	Time	Size (Bytes)
/	RockFallOnWP_Plots.xls	7/5/2007	2:34pm	2,856,960
/Case01	d3hsp	3/8/2007	10:21am	91,515,357
	tada2m1b_coarse.k	3/7/2007	6:10pm	8,386
	tada2m1b_coarse.inc	3/8/2007	10:21am	27,447,417
	tada2m1b_coarse.tg	3/8/2007	10:21am	70,864
/Case02	d3hsp	3/8/2007	10:20am	134,348,633
	tada2m1b_std.k	3/7/2007	6:12pm	8,387
	tada2m1b_std.inc	3/8/2007	10:20am	41,554,053
	tada2m1b_std.tg	3/8/2007	10:20am	70,852
/Case03	d3hsp	3/8/2007	10:18am	170,423,989
	tada2m1b_refined.k	3/7/2007	6:13pm	8,427
	test.stdout	3/7/2007	6:13pm	20,254
	tada2m1b_refined.tg	3/8/2007	10:17am	70,832
	tada2m1b_refined.inc	3/8/2007	10:17am	53,154,839
/Case04	tada2m1b.tg	3/7/2007	6:14pm	70,832
	tada2m1b.k	3/7/2007	6:14pm	8,391
	d3hsp	3/8/2007	9:50am	161,712,349
	tada2m1b.inc	3/8/2007	9:49am	50,326,703
/Case04/Case04a	d3hsp	3/8/2007	10:12am	162,201,544
	tada2m1_IVbot.k	3/7/2007	6:19pm	8,194
	test.stdout	3/7/2007	6:19pm	20,096
	tada2m1_IVbot.tg	3/8/2007	10:12am	70,941
	tada2m1_IVbot.inc	3/8/2007	10:14am	50,326,999
/Case05	d3hsp	3/8/2007	10:23am	157,127,916
	tad_a1m1q1.k	3/7/2007	6:20pm	8,456
	test.stdout	3/7/2007	6:20pm	20,440
	tad_a1m1q1.inc	3/8/2007	10:23am	47,856,476
	tad_a1m1q1.tg	3/8/2007	10:23am	74,953
/Case06	d3hsp	3/8/2007	10:25am	185,795,727
	tad_a1m8_mid2e.k	3/7/2007	6:21pm	8,539
	tad_a1m8_mid2e.inc	3/8/2007	10:24am	53,229,175
	tad_a1m8_mid2e.tg	3/8/2007	10:24am	81,639
/Case06/Case06a	d3hsp	7/5/2007	10:23am	165,336,911
	tad_a1m8_mid2d_21PWRa.k	5/14/2007	11:04am	9,073
	test.stdout	5/14/2007	11:05am	15,144
	tad_a1m8_mid2d_21PWRa.tg	5/14/2007	11:04am	88,972
	tad_a1m8_mid2d_21PWRa.inc	7/5/2007	10:20am	53,332,021

/Case07	d3hsp	3/8/2007	10:28am	174,401,053
	tada1m1tb.k	3/7/2007	6:23pm	8,468
	test.stdout	3/7/2007	6:23pm	19,182
	tada1m1tb.tg	3/8/2007	10:28am	73,686
	tada1m1tb.inc	3/8/2007	10:28am	54,233,712
/Case08	TADa2m9b.k	3/7/2007	6:24pm	8,188
	TADa2m9b.tg	3/8/2007	10:30am	70,890
	TADa2m9b.inc	3/8/2007	10:30am	54,463,091
	d3hsp	3/8/2007	10:30am	169,669,060
/Case08/Case08a	TADa2m9b_noCorr.tg	5/14/2007	11:02am	71,291
	TADa2m9b_noCorr.inc	7/5/2007	10:46am	54,445,150
	TADa2m9b_noCorr.k	5/14/2007	11:02am	8,201
	d3hsp	7/5/2007	10:46am	161,331,243
	test.stdout	5/14/2007	11:05am	19,611
/Case09	TADa2m1bolt4.k	3/7/2007	6:25pm	10,085
	TADa2m1bolt4.tg	3/8/2007	10:30am	90,585
	TADa2m1bolt4.inc	3/8/2007	10:31am	80,764,950
	d3hsp	3/8/2007	10:32am	242,066,762
/Case10	TAD_a1m1qbolta2.k	3/7/2007	6:25pm	8,842
	TAD_a1m1qbolta.tg	3/8/2007	10:32am	92,435
	TAD_a1m1qbolta2.inc	3/8/2007	10:33am	73,333,617
	d3hsp	3/8/2007	10:33am	240,304,949
/Case11	TADa1m8bolt_mid2f.k	3/7/2007	6:26pm	9,609
	TADa1m8bolt_mid2f.tg	3/7/2007	6:33pm	100,314
	TADa1m8bolt_mid2f.inc	3/8/2007	10:34am	66,776,018
	d3hsp	3/8/2007	10:34am	214,368,464
/Case12	TAD_a1m1tboltc.k	3/7/2007	6:27pm	10,591
	test.stdout	3/7/2007	6:27pm	27,099
	TAD_a1m1tboltc.tg	3/8/2007	10:36am	91,293
	TAD_a1m1tboltc.inc	3/8/2007	10:37am	75,814,021
	d3hsp	3/8/2007	10:37am	234,023,186
/Case13	tada2m1b_dbl.tg	3/7/2007	6:28pm	73,700
	tada2m1b_dbl.k	3/7/2007	6:28pm	8,521
	d3hsp	3/8/2007	10:38am	172,170,452
	tada2m1b_dbl.inc	3/8/2007	10:38am	53,669,421
/Case14	TADa2m1bolt4b_multi_2.k	3/7/2007	6:29pm	10,097
	TADa2m1bolt4b_multi_2.tg	3/7/2007	6:33pm	92,413
	TADa2m1bolt4b_multi_2.inc	3/8/2007	10:39am	57,780,285
	d3hsp	3/8/2007	10:40am	176,465,197
/Case15	5dhlwa2m1.tg	3/7/2007	6:30pm	82,034
	5dhlwa2m1.k	3/7/2007	6:30pm	8,977
	d3hsp	3/8/2007	10:41am	152,348,710
	5dhlwa2m1.inc	3/8/2007	10:40am	49,302,930
/Case16	5dhlwa2m1_newSleeve.k	3/7/2007	6:31pm	8,987
	test.stdout	3/7/2007	6:31pm	20,549
	d3hsp	3/8/2007	10:41am	163,985,724
	5dhlwa2m1_newSleeve.tg	3/8/2007	10:41am	82,054
	5dhlwa2m1_newSleeve.inc	3/8/2007	10:41am	53,418,855

Note: File sizes may vary with operating system

ATTACHMENT II.
FIGURES OBTAINED FROM LS-DYNA

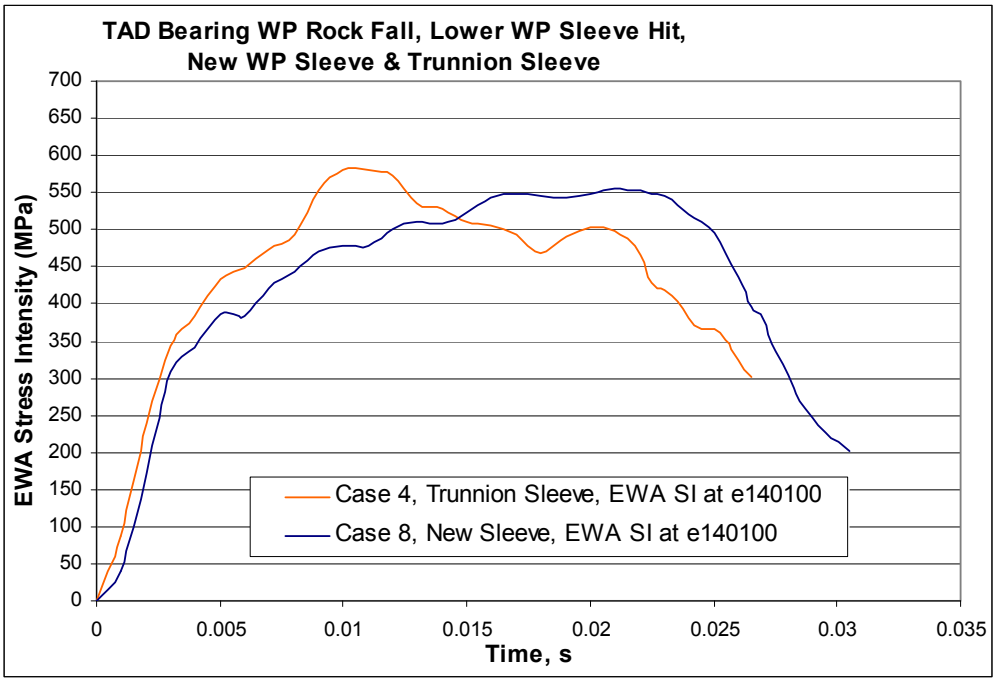

Figure 14. Effect of Sleeve Geometry, Lower Sleeve Rock Fall, EWA Stress Intensity, OCB Lower Lid, 20 MT (22 ton) Rock Fall at 10 m/s (32.8 ft/s) (Case #4 and #8)

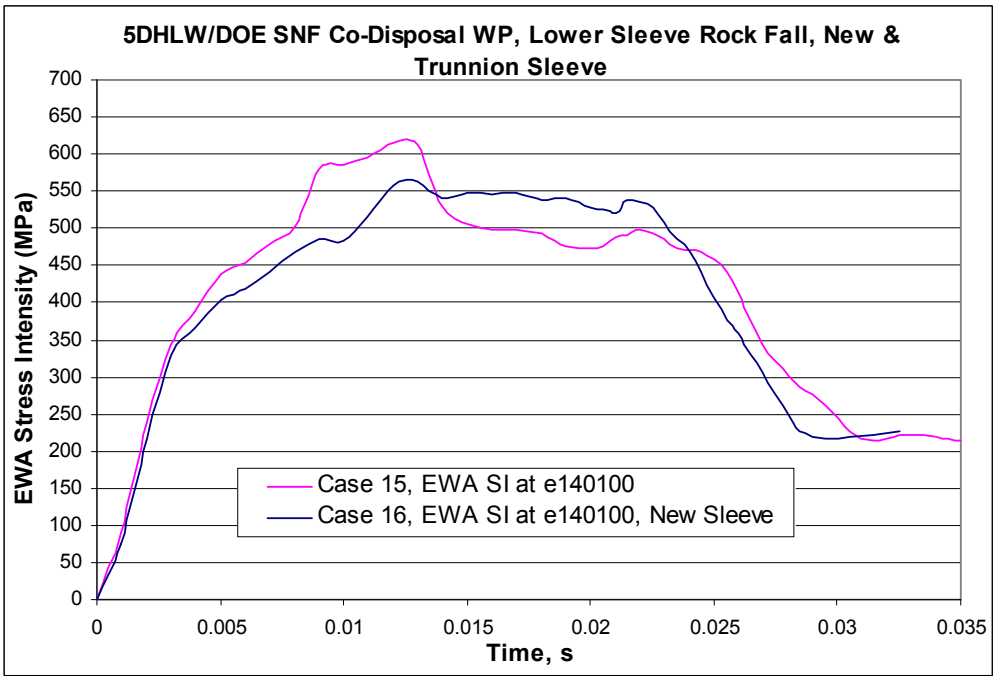

Figure 15. Effect of Sleeve Geometry, Co-Disposal WP Lower Sleeve Rock Falls, EWA Stress Intensity, OCB Lower Lid, 20 MT (22 ton) Rock Fall at 10 m/s (32.8 ft/s) (Case #15 and #16)

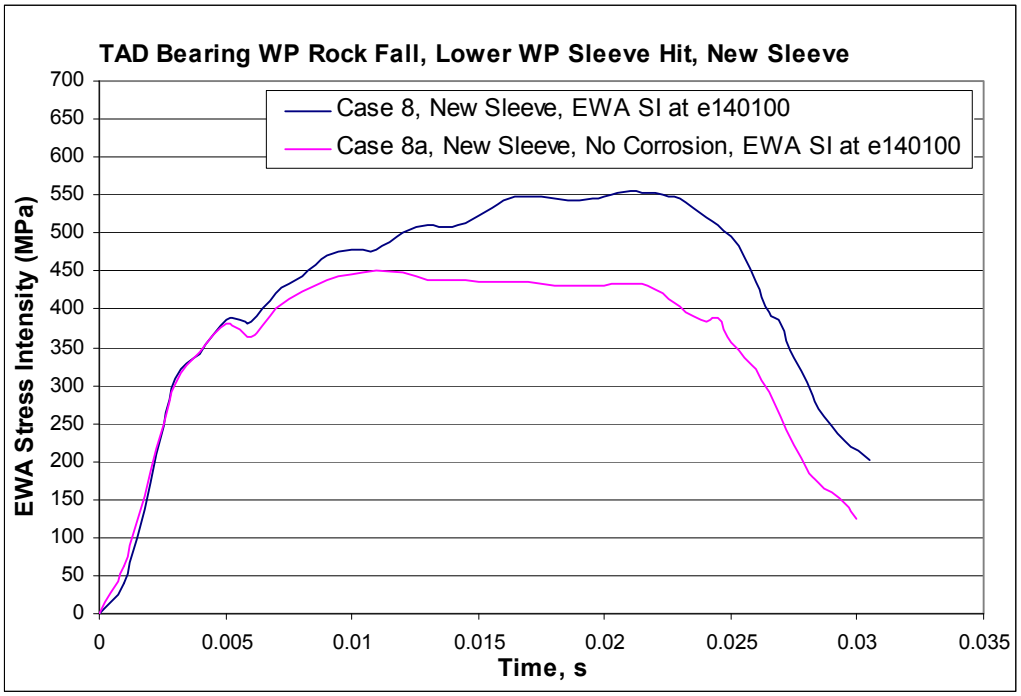

Figure 16. Effect of Corrosion Condition, EWA Stress Intensity, OCB Lower Lid, 20 MT (22 ton) Rock Fall at 10 m/s (32.8 ft/s) (Case #8 and #8a)

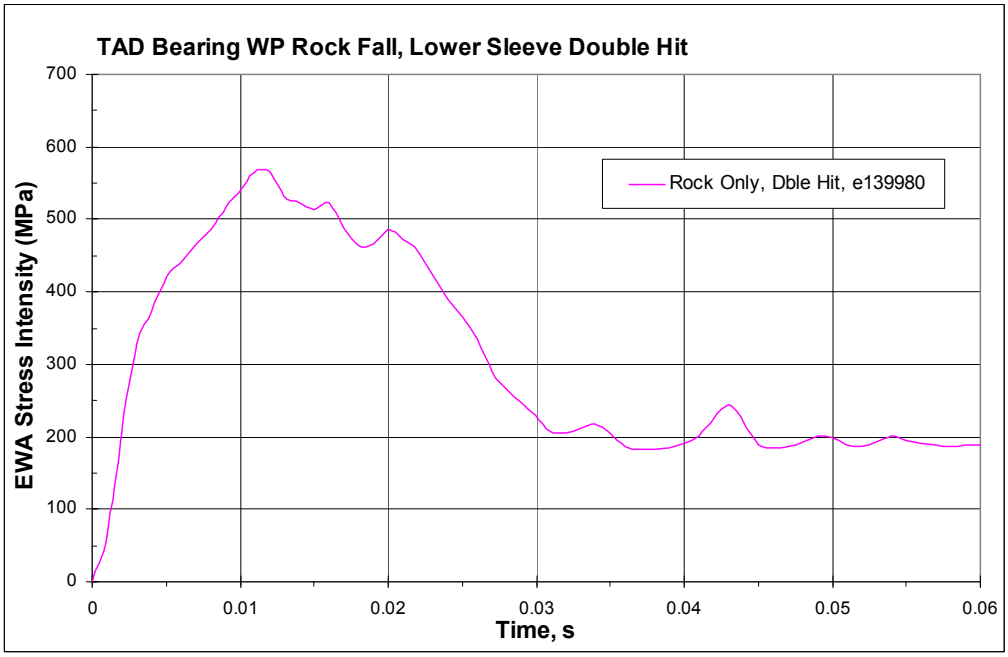

Figure 17. Effect of Double Hit, EWA Stress Intensity, OCB Lower Lid, Maximum 20 MT (22 ton) Rock Followed by a 0.5 MT (0.55 ton) Rock (Case #13)

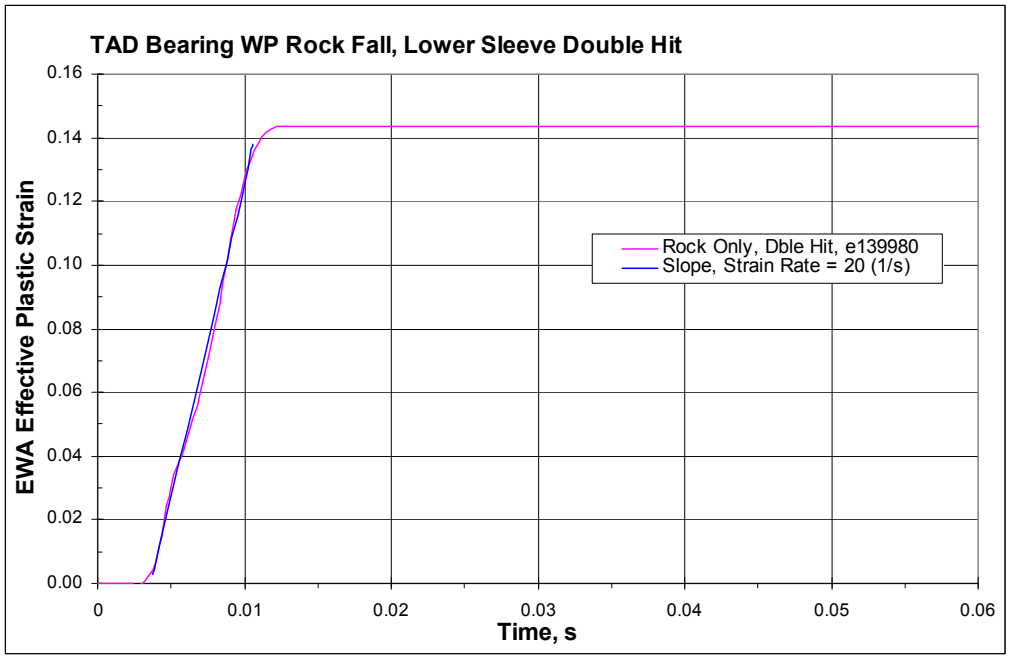

Figure 18. Effect of Double Hit, Effective Plastic Strain, OCB Lower Lid, Maximum 20 MT (22 ton) Rock Followed by a 0.5 MT (0.55 ton) Rock (Case #13)

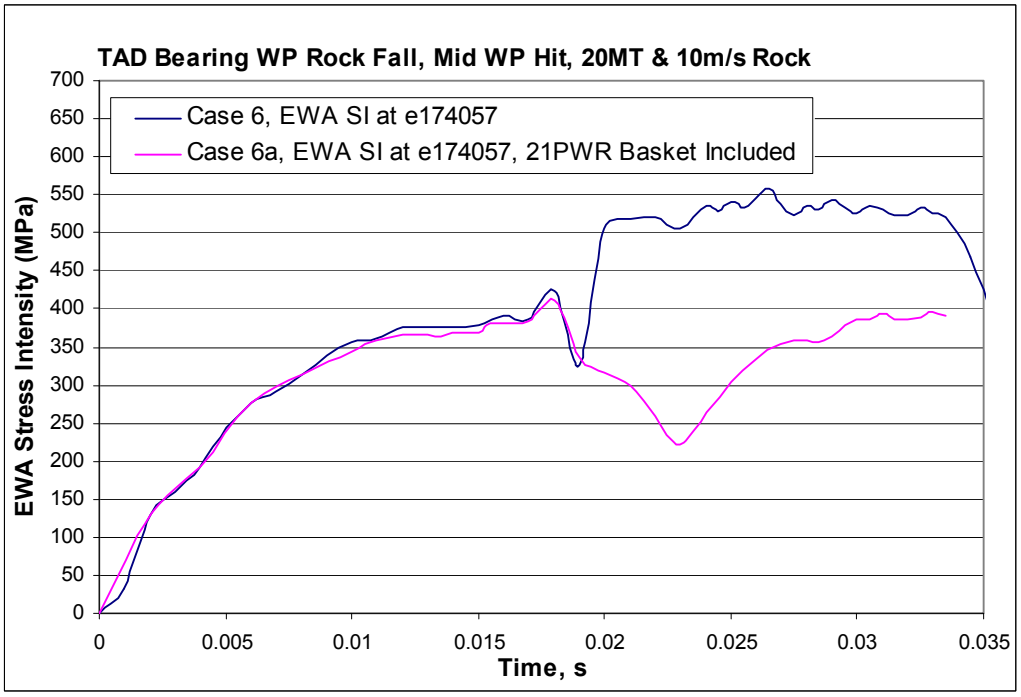

Figure 19. Effect of Internals, TAD Bearing WP, Mid Package Rock Fall, EWA Stress Intensity, 20 MT (22 ton) Rock Fall at 10 m/s (32.8 ft/s) (Case #6 and #6a)